ADDIS ABABA UNIVERSITY

SCHOOL OF GRADUATE STUDIES

ADDIS ABABA INSTITUTE OF TECHNOLOGY

SCHOOL OF MECHANICAL AND INDUSTRIAL ENGINEERING

Investigation on Crashworthiness of Locally Manufactured Bus structural frame by using Numerical Approach

A Thesis Submitted for the Partial fulfillment of the requirements for the Degree of Master of Science(M.Sc) in Mechanical Engineering (Mechanical Design) to the School of Mechanical and Industrial Engineering, Addis Ababa Institute of Technology, Addis Ababa University

By

Alazar Mulugeta

Advisor

Haileleoul Sahle Habte (PhD)

December, 2021

Declaration

I hereby declare that this submission is my own work and to the best of my knowledge it contains no materials previously published or written by another person, or substantial proportions of material which have been accepted for the award of any other degree or diploma at Addis Ababa University or any other educational institution, except where due acknowledgement is made in the thesis.

Name: Alazar Mulugeta Woldetsadik

Place: Addis Ababa, Ethiopia

Date of submission: _____

Signature: _____

Title of the thesis:

Investigation on Crashworthiness of Locally Manufactured Bus structural frame by using Numerical Approach

This thesis has been presented for examination with my approval as a university advisor.

Dr. Haileleoul Sahle Habte _____ _____

Advisor Signature Date

ADDIS ABABA UNIVERSITY

SCHOOL OF GRADUATE STUDIES

ADDIS ABABA INSTITUTE OF TECHNOLOGY

SCHOOL OF MECHANICAL AND INDUSTRIAL ENGINEERING

Investigation on Crashworthiness of Locally Manufactured Bus structural frame by using Numerical Approach

By:

Alazar Mulugeta Woldetsadik

Approved by Board of Examiners:

Dr. Haileleoul Sahle Advisor	_____ Signature	_____ Date
Dr. Araya Abera Internal Examiner	_____ Signature	_____ Date
Dr. Mulugeta Habtemariam External Examiner	_____ Signature	_____ Date
Dr. Yilma Tadesse SMIE Dean	_____ Signature	_____ Date
Dr. Ermias Tesfaye Post-Graduate Program Director	_____ Signature	_____ Date

Acknowledgment

First and foremost, I would like to thank almighty God: for all things are done because of him.

I would like to express profound gratitude to my advisor and teacher, Dr. Haileloul Sahle, for your patience, guidance, and support. You have been an ideal teacher, mentor, and thesis advisor. I am grateful for your wealth of knowledge and meticulous editing.

A special thanks go to the teaching staff of mechanical engineering department for their continuous support.

Last but not least, I would like to thank my family for their support and encouragement.

Abstract

The thesis aimed to investigate the crashing behavior of locally manufactured 60 seated bus structural frames in case of frontal and side impacts. In addition to studying the crashworthiness of current structure, the most severe impact condition was identified by referring to crash test and an improvement on structure for a better crash performance for that impact condition was proposed.

A full frontal and an offset impact position were used for frontal impact testing while analysis for side impact a perpendicular and angled/oblique impact position were used. Full-frontal crash analysis was done according to the ECE-R29 involving a frontal crash pendulum test in which impacting energy is set to 55 kJ and safe space between steering model and manikin is checked. while for offset frontal impact a simulation of bus structure impacting a rigid wall with an initial velocity of 56km/hr was done to check structures response to such kind of accidents. For side-impact, residual space specified on ECE-R60 was used to check side frame deformation in case of perpendicular and angled/oblique impact. An impacting trolley with an initial speed of 48 km/hr was used for the side-impact test.

Commercial software CATIA and ABAQUS were used for geometrical modelling and analysis. The study focused on identifying the crashworthiness of the bus structure by analyzing the structural deformation, crash pulse, crash force efficiency, HIC, and energy absorbing capacity.

The results showed that the current structure had failed to meet regulation in the case of both frontal impacts and side perpendicular impact. In full frontal impact an intrusion of 17.32 mm in to manikin is seen and side frame has intruded residual space by 8.22 mm. Amongst the tests most severe impact damages was observed in the case of full-frontal and off-set frontal crash tests.

For improving crashworthiness of the structure, three models were proposed and tested according to ECE-R29, the first two were based on increasing the thickness of frames and the last was by adding a reinforcement profile. The simulation results for improved models showed, by adding a reinforcement profile has improved the crashworthiness of the bus by creating a space between manikin and steering model of 36.33 mm structure and meets with regulation.

Keywords: Crashworthiness, locally developed 60 seat bus, Frontal impact, Side impact, Dynamic/ explicit analysis, optimization

TABLE OF CONTENTS

List of Tables

List of Figures

Glossary

3D	: Three Dimensional
ADR	: Australian Design Rule
C3D4	: 4-Node Linear Tetrahedral Element
CAD	: Computer-Aided Design
CAE	: Computer-Aided Engineering
CFE	: Crash Force Efficiency
CPU	: Central Processing Unit
E.C	: Ethiopian Calendar
ECE	: Economic Commission for Europe
FE	: Finite Element
FEA	: Finite Element Analysis
FEM	: Finite Element Method
FMVSS	: Federal Motor Vehicle Safety Standards and Regulation
HIC	: Head Injury Criterion
LMS	: Lamped Mass System
PLC	: Private Limited Company
R	: Regulation
RHS	: Rectangular Hollow Sections
SEA	: Specific Energy Absorption

CHAPTER ONE:

1. Introduction

1.1. Background of the study

Since mankind has started using a man-made transportation system there has been a lot of innovations and improvements done. Among the different transportation means available, bus transportation is the one which is used as the most common mass transportation worldwide due to its convenience and low cost. Most buses in use in Ethiopia are made by locally modifying the imported trucks. Manufacturing of body structure for mass transportation vehicles in Ethiopia is estimated to start by making locally known “wuyiyit” locally used as taxis, which are built upon most pick-up vehicles [1]. Local manufacturers built the structure of the buses on top of the chassis and power train of imported trucks.

Most local companies currently manufacturing bus bodies use the sub-frame and power transmission of trucks models like ISUZU NPR, ISUZU FSR, ISUZU FVR, MERCEDES, IVECO, DAEWOO, and sometimes well-known buses (like TATA) are rebuilt by using local materials after they encounter an accident or when their body is worn due to age. Some builders use imported chassis and power trains of Daewoo and Mercedes buses, which are already designed and prepared for bus body building. The manufacturing method for different bus models and sizes is mostly the same with modifications in dimensions and number of structural components. Some of the well-known 60 seated bus body builders are ADA Engineering PLC, Orbis motors S.C, Ultimate motors PLC, ANTA Engineering PLC, and Maru PLC.

The body structure of the locally manufactured bus is constructed from welded RHS frame, which consists of six sections of the roof, two side bodies, frontal structure, and floor member. Those frames are welded on continuous longitudinal members attached to the chassis using welding and some reinforcement by using bolts. The design and manufacturing of buses should be based on structural stability, lightweight, and mainly crash tests, which should be monitored by bus producers and local administration. From data and interviews made with local bus body builders, the main requirements imposed by local authorities are on general size, seating position and distance between seats, inner ceiling to roof distance, and ground clearance only. With no requirements regarding crashworthiness and vehicle weight [1].

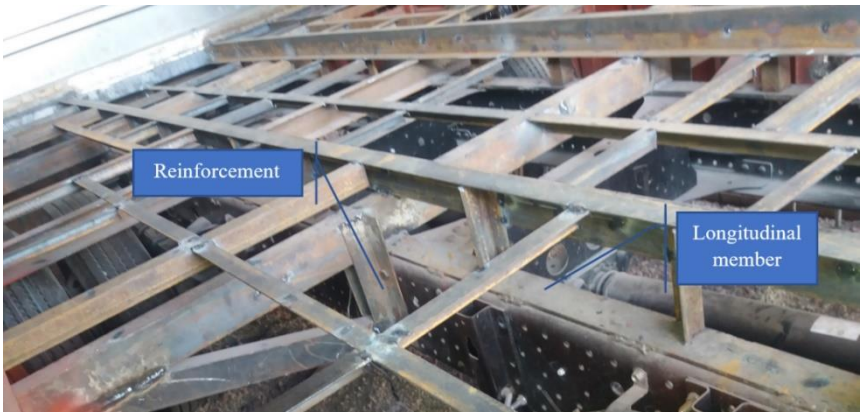

Figure 1-1, Floor assembly of a locally manufactured bus

Because such buses carry a minimum of 24 passengers and up to 60 passengers, the total amount of people at risk when a bus encounter an accident is high. Properly designed and manufactured bus structure will help in protecting occupants during accidents. Analyzing the crashworthiness will show if the current method used is adequate in achieving this goal. In this research, two types of bus accidents are considered for investigation. One is frontal impact and the other is side impact.

Front-impact accidents are one of the frequent types of accidents observed in vehicles. It is mostly caused during emergency braking. During such kinds of accidents occupants inside the bus can get injured due to the impact with the handrail, seat, and other body parts.

Figure 1-2, Frontal impact to locally manufactured DAEWOO

Side impacts are not as common as frontal impacts, they are mostly caused when two vehicles collide. In such kind of accident as passengers are much closer to the impact area, the structure should be able to absorb the energy developed during impact and should not deform beyond the

desired range. In addition, side doors should be able to stay locked during and after impact to protect occupants from falling out of the bus.

The crash worthiness of locally manufactured buses, in Ethiopia, has not been properly studied. In this study, numerical analysis is targeted to study the crashworthiness of locally manufactured bus structure during frontal and side-impact.

1.2. Statement of the problem

Alarmingly increasing road accidents in Ethiopia have led to the death and injuries of many lives. Especially accident to long traveling buses has taken the life of many people. Most insurance company history on bus accidents shows that passengers are severely injured during accidents. The most commonly used type of locally manufactured 60-seater bused in use are Iveco, Deawoo, and Mercedes buses. Currently, Deawoo and Mercedes buses are mostly being preferred by manufacturers.

The locally manufacturing bus bodies have larger demand compared to foreign imported buses[1]. Their methods and procedures have with time increased with little improvement in their design and manufacturing method. The main criteria's that authorities impose are regarding total height and width of the bus, door size, ground clearance, inner roof distance, size and distance of chairs, and other parameters in regard to clearance only. With those requirements stated, local bus body builders have given less emphasis on structural stability, weight and load carrying capacity. Site visits conducted at different bus bodybuilders in Addis Ababa, it was observed that the manufacturing method doesn't follow any known regulation or standards in regards to crashworthiness. In addition, the structure of the bus should be able to properly absorb the energy developed during impact and deform in a controlled way to decrease injuries to passengers.

The requirement for structures response to crash are not properly stated and measured by using numerical or an experimental approach. One MSc thesis Research is carried out in AAiT regarding crashworthiness of mid-bus (24-seater bus) in case of a rollover accident by Hailemechel. Proper testing of crashworthiness of locally manufactured buses in the case of Frontal and side-impact has not yet been studied. In this thesis crashworthiness of locally manufactured 60 set bus is studied in case of frontal impact and side impact accidents.

1.3. Objectives of the Study

1.3.1. General objective

The main objective of this study is to investigate the crashing behavior of locally manufactured 60-seated bus structural frames for frontal and side crashes by using finite element (FE) method.

1.3.2. Specific objective

- Conduct numerical analysis to determine the crashing behavior of the structure.
- Investigate the deformation of structure for severe conditions.
- Investigate the energy absorbing capacity of the structure in the case of frontal and side-impact conditions.
- Investigate the crash pulse of the structure for severe impact conditions.
- To identify severe impact position and come up with a new proposal to enhance the crashworthiness of the locally developed 60 seated bus.

1.4. Significance of the Study

Evaluating the crashworthiness of locally manufactured bus structure will help in insuring occupants' safety. The finding of this study will help to inform bus manufacturers on the crashworthiness of their bus structure and show some improvement methods. Also, the study will give an initial platform for designing and manufacturing a bus structure concerning crashworthiness.

This study may be of great benefit to the National transport authorities of Ethiopia, amongst other stakeholders, as they seek to address road safety. As the study shows the crashworthiness of the current bus structure, they can use the finding to enforce legislations and regulations in regards to a more crashworthy structure.

The immediate beneficiaries are mostly the driver and passengers of locally manufactured buses. As most causalities that occur due to road accidents are to occupants [2], developing a more crashworthy structure help in reducing injuries and increasing safety. It's hoped that the concerned authorities and bus body manufactures will make the right decision with regards to the safety of locally manufactured buses in our country after reviewing this study. It also will serve as an additional benchmark for future researches regarding locally manufactured buses.

1.5. Scope and Delimitations of the Study

1.5.1. Scope of the Study

The study focuses on studying the crashworthiness of locally manufactured 60-seater DAEWOO bus structural frame against frontal and side-impact accidents. Geometrical modeling is done by using CATIA and the "iges" file is imported to ABAQUS for numerical simulation. the dimensions of structure and materials used are taken by direct measurement at local bus manufacturer. The numerical analysis is done by using explicit dynamic FEA. The results for deformation, energy absorption, crash force, and crash pulse are used to determine the crashworthiness of the structure by comparing with regulations stated in this thesis. Finally, after analyzing the crash behavior in both impact scenarios a possible improvement is proposed for the severe impact position.

1.5.2. Delimitations of the Study

As mentioned in the introduction section, there are different types of accidents, and the structure responses for each type of impact are different. In this study, the structure response for frontal and side-impact are only taken for analysis.

To have a clear understanding of the crashworthiness of any structure, it is a must to conduct an experimental test on the full size or section of the structure. Due to lack of finance and willing funder to conduct such kind of experiment at this stage, only simulation is done.

Structural failure due to improper welding is not taken into consideration. All welding joints are assumed to be perfectly welded with no defects.

In a side- test, an impacting trolley is used to simulate a vehicle hitting a bus from the side. The standard recommends using a deformable part, mechanical fome, impactor. For sake of simplicity and decreasing simulation time. The impacting trolley is modeled as a rigid body, while other parameters are per regulations.

1.6. The expected output of the study

At the end of this study, the crashworthiness of a locally manufactured 60-seater bus structure is discussed by analyzing the deformation range, energy absorbing capacity, crash pulse, HIC, and crash force in case of frontal and side impact. The results are going to be used for determining the crashing behavior of the current structure based on internationally known and accepted regulations.

1.7. Organization of the thesis

This thesis consists of six chapters, the present chapter (Chapter-1) Made an introduction to the problem to be studied in this thesis, and the main and specific objectives are outlined.

Chapter-2, Review of literature regarding crashworthiness of bus structure is made and description of the basic testing parameters are discussed.

Chapter-3, Mathematical model regarding FEA is shown and some of the simulation methods are discussed in detail. The chapter concludes by showing the simulations method for testing the crashworthiness of bus structure according to selected regulations.

Chapter-4, Finite element modeling of the structure starting from geometrical modeling, and FE analysis setup is shown.

Chapter-5, The results from FEA are displayed and discussed in detail by using figures, charts, and tables. Finally, an improvement on the crashworthiness of the current structure is proposed.

Chapter-6, Provides the conclusion, recommendations, and future work.

CHAPTER TWO:

2. Literature review

Many severe road traffic accidents in Ethiopia involve public transport vehicles. Up to 35.42% percent of fatal crashes occur due to buses [2]. The fatality rate to such type of vehicle is high due to fact that most populations rely on public transportation. Amongst all death resulting from accidents, occupants are the most vulnerable accounting for nearly 52% of road death in 2018 [2]. With the majority of death occurring to occupants of buses, safety futures and structure play a great role in decreasing the injury rate.

The major development method of bus structure is by welding thin-walled tubes. Such tubes are widely used in bus body structure because of their high specific energy absorption, stable deformation mode, and lightweight characteristics [3]. In addition, thin-walled tubes are easy to assemble and weld together. Construction of bus body frame by using those tubes is most commonly used throughout the world.

With site visits done at various bus manufactures, the manufacturing methods are seen to be based on experience only with no proper design and guideline. The design and manufacturing of buses should be based on structural stability, strength, and crash resistance to ensure occupants' safety [3]. In any accident scenario, if the structure of the bus doesn't absorb the kinetic energy due to impact/collision occupants have a high risk of being injured or even death will be inevitable. In addition to absorbing the energy, the magnitude of deformation will contribute greatly in resulting severe injuries to occupants.

Possible injuries to occupants can be predicted by analyzing the deformation characteristics of structures intrusion into inner sections of the bus (occupants area) during and after a crash [4]. Different sections of bus structure are responsible for protecting occupants from injuries for different accident scenarios like frontal collision, side collision, rear collision, and rollover.

2.1. Theoretical background

2.1.1. Accident Types

2.1.1.1. Frontal collision

Frontal impact is the major cause of accident among all bus accidents. Such accidents cause great injury and fatalities to drivers and occupants. During impact, the absorbed kinetic energy is dissipated into the deformation of the structure. This will cause occupants and other items

inside to move freely if not properly restrained. If occupants and other items are properly constrained the energy will be transferred to the structure. The remaining energy will be dissipated by the deceleration of the bus.

If the impact loading is higher than the safety limit occupants will sustain injuries resulting from internal vehicle body parts or uncontrolled body motion. A proper design should absorb and ensure gradual dissipation of kinetic energy through vehicle structure and reduce injuries.

By physical inspection of frontal collision accidents, we can mainly categorize them by using the position of impact as full-frontal collision and offset frontal collision.

In case of a full-frontal collision, the front section of the bus is in total contact with the impacting object. Such kind of collision commonly occurs when the bus collides with a wall, or some type of large solid object, heavy trucks and buses, and the like. In such cases, the whole front structure of the bus is damaged and deformed. Figures 1-2 show a real case full-frontal collision.

In offset frontal collision either in the driver compartment or passenger side, the main components of the bus structure under load are the side pillars. Because the front section of the bus has doors on both sides the side pillars are highly affected by the collision, which might result in injuries to occupants. Figure 2-1 shows damaged buses due to offset frontal collision.

Figure 2-1, Frontal offset collision

2.1.1.2. Side collision

Side impact is commonly caused when a striking vehicle hits another vehicle in the left-hand or right-hand side of the bus body. The kinetic energy is dissipated to both vehicles resulting in the deformation of both vehicle bodies. The process of side impact can be categorized into two stages as described in a frontal impact. Unlike frontal impact, restraints play less role in protecting occupants from injury as they are close to side structure and doors. Hence, the strength, layout, and stiffness of the side structure play a major role in minimizing occupants' injuries.

Figure 2-2, Side impact of bus

2.1.1.3. Rear collision

Though the number and severity of rear impacts are less than the number of frontal and side impacts, the whiplash injuries caused by such types of accidents are complicated, hard to recover from, and can cause fatalities. For rear impact, special infancies are considered for structural stability of head restraints, seatbacks, and safety of fuel tank and fuel lines.

Figure 2-3, Rear collision

2.1.1.4. Rollover

Roll over can be caused while a vehicle, due to a strong collision or instability tumbles. During this accident, the whole vehicle structure should be able to protect occupants from injuries. Rollover accidents are one of the most severe accidents in respect of occupants' injuries and fatality levels. Especially in buses due to their high number of occupants and size the structure should be adequate to protect occupants' safety and decrease injuries. The structural parts like pillars, luggage racks, reinforcement, and other internal components shouldn't rack outside the residual space.

Figure 2-4, Rollover accident

2.1.2. Motor Vehicle Safety

Automotive safety is the study and practice of design, construction, equipment, and regulation to minimize the occurrence and consequences of traffic collisions involving motor vehicles, road traffic safety more broadly includes roadway design . The birth of automotive safety was due to the first motor vehicle accident resulting in death to occupants, which occurred in 1889 in New York City. This event led to the birth of automotive safety as a field of study [5]. From the first birth of automotive safety study, the progress in protection system and safety design can be labeled into three different periods in the development history of the field.

At early stages, the main focus was to reduce accidents/collisions that occur due to an abnormal operating condition of vehicles. For example, reduction on tire blowouts, self-starter engines, head lamps, laminated glass, and adopting an all-steel body structure. This improvement had reduced some injuries and accidents. In addition, the first full-scale crash test was conducted involving rollover simulation and car-to barrier impact .

In the second stage, automotive manufacturers introduce crash avoidance devices like signal lamps, windshield glass wipers, the first head impact simulation to the dashboard, and many other improved safety futures which can reduce fatality accidents. One of the main safety devices of that time was the introduction of seat belts as an option in 1956. In addition, General Motors conducted the first car-to-barrier frontal crash test.

In today's modern world, the main transportation safety effort focuses on crashworthiness, crash avoidance, driver performance, and highway construction [6]. Over the past years, many safety features were added to automobiles to avoid crash, such as anti-brake systems and traction control.

The design of automotive safety features are categories in to active and passive safety systems [7]. Active systems are designed to prevent accidents. Some of the basic and most common active systems are brake, traction control system, antilock brake system, and Electronic stability program. These systems are designed to stop the vehicle properly without causing an accident. But they are not always effective, the systems may fail due to many reasons like poor maintenance, improper design, and other external factors. In addition, accidents are unpredictable which will result in misusage by the driver resulting in collision or overturning. From the moment of the first impact up to complete stop of the vehicle is addressed by using passive safety. Passive safety systems are mainly designed and used to decrease injuries to occupants. In passive safety stage safety devices like air bags, seat belts, pedestrian passive safety systems, and automobile structures will protect occupants. Table 2-1 summarizes the main categories of vehicle safety systems.

Active System	Passive System
• Brake • Traction control system • Anti-lock braking system • Electronic stability program	• Seat belt • Air bag • Active hood • Pedestrain passive safety system • Vehicle structure

Table 2-1, Vehicle Safety Systems

2.1.3. Crashworthiness

Crashworthiness is the measure of the ability of a structure and its components to protect its occupants during a survivable crash [8]. In automotive industry, it measures the structural ability to physically deform by maintaining sufficient survival space for occupants during a crash involving a reasonable deceleration load.

2.1.3.1. Crash characteristics

Accidents to an automobile can occur in different manners and speeds. The accident may be due to Front impact with a stationary object, automobile to automobile impact, rollover, and collision with a pedestrian. The structure of an automobile is differently affected depending on the extent and nature of the accident. For example, a frontal impact with stationary objects like rigid barriers, trees, light poles, and the like will severely decelerate it causing high impact load [9]. Crashworthiness can be characterized by using crash pulse, crash position, displacement and energy, and automobile capability. In addition to predicting the motion of occupants, the characteristics of the measured crash pulse will show the crashworthiness of the vehicle. The value must be less than a certain limit set by regulations. The crash pulse of the structure will show the automobile's capability to mitigate severe injury that might be caused by different positions of crash such as side-impact, rollover, offset frontal impact, rear impact, and full-frontal impact.

In modern vehicle design frontal structure is being shortened for design value and still is required to sustain high impact energy and distribute the load to other structural parts. For different models, the structure should be capable of reducing injuries to occupants during accidents involving two different automobiles.

2.1.3.2. Crashworthiness requirements

Vehicle structures should sufficiently stiff in bending and torsion for proper ride and handling. The structure should be able to minimize high frequency vibration and decrease deceleration pulse which could occur during an accident. The structure should possess the following properties to yield satisfactory deceleration pulse to accommodate passengers' size, ages and crash speeds for both genders [8].

- Deformable, yet stiff, front structure with crumple zones is expected to absorb the kinetic energy resulting from the frontal collisions by plastic deformation and prevent

intrusion into the occupants' compartment, especially in case of offset crashes and collision with narrow objects such as trees.

- Deformable rear structure to maintain the integrity of the rear passenger compartment and protect the fuel tank.
- Properly designed side structures and doors to minimize intrusion in side-impact and prevent doors from opening due to crash loads.
- Strong roof structure for rollover protection.
- Properly designed restraint system that works in harmony with the vehicle structure to provide the occupant with an optimal ride down and protection in different interior spaces and trims.
- Accommodate various chassis designs for different power train locations and drive configurations.

To check if vehicles achieve the above requirements different experimental tests should be done. Although properly modeled FEA gives an accurate result laboratory tests are mandatory in regards to vehicle certifications. The testing methods are mainly done in three categories as components test, sled test, and full-scale test [3]. Due to the expensiveness of conducting a repeated analysis of full-scale barrier tests most experimental tests rely on component tests. This test determines the dynamic or quasi-static response to the loading of an isolated component. Conducting such kinds of tests is best in identifying the crash mode and energy absorption capacity.

2.1.4. Crash pulse

Crash pulse shows the deceleration time history at a point in the vehicle during impact [10]. Crash pulse on side pillars or total motion in case of frontal impact will help identify the crashworthiness of the structure. The nature of the crash response of any given vehicle depends on the mass, structural stiffness, damping behavior of the structure, and external loading condition. A crash pulse curve can be used to assess the severity of an occupant's injury. The shape, time duration, and maximum acceleration of crash pulse can be used to analyze the crashworthiness of a vehicle [10]. Crash pulse is one of the useful types of data for describing what occurs to the structure of vehicle in crash and can be used to determine how occupants react to a crash.

Crash pulse measures energy variation during the impact and can be directly related to occupants' injuries. Crash pulse can be used to find head injury criteria (HIC), HIC is the most

important parameter in terms of human survival; it is indicative of brain injuries due to the impact of the head in numerous cases [11].

2.1.5. Vehicle crash modelling

Deceleration time history of vehicle structure during accident and knowledge of their interaction with occupants is necessary for the crash-worthy design. Effective methods and tools are necessary to enable the initiation of a sound design at the early concept phases of development. Currently, the design process relies on calculating the crash pulse from either Lumped Mass-Spring (LMS) models or Finite Element (FE) models [3].

Lamped parameter models: initially developed in 1970 by (Kamal) is a simple but powerful model for simulating the crashworthiness response of a vehicle for frontal impact. The model is widely used by crash engineers due to its simplicity and relatively accurate result. It's one of the first numerical analysis methods used for crashworthiness analysis by using a one-dimensional model. LMS is useful in developing vehicle structure for a crash and helps the design process by calculating the crash pulse. LMS relied on a static crash test to establish the spring stiffness. The main limitation in LMS model is one-dimensional and analysis requires prior knowledge of spring characteristics.

Nonlinear Finite element models: During impact, structural components of the bus undergo a large deformation following in high stress. Afterwards, as the stress exceeds material yielding stress limit it results in a large progressive elastic-plastic deformation. For such kind of loading non-linear finite element method is best used in determining the crashing behaviors of automotive structures[4]. Most commercial software used to solve FEM are developed to solve such kind of problems by using the following steps.

- **Pre-Processing**: Modeling, application of load and boundary conditions.
- **Solving**: Solves the finite element function by using a specified solver and outputs the data
- **Post-Processing**: Outputs data and visualizes the results

Thera are different types of numerical simulation software being used for FEA. Currently, ABAQUS, PAM-CRASH, ADINA, CRASH CAD, ANSYS, RAIOS and LS-DYNA are widely used for crash simulation. Crash analysis simulation and results can be used to asses crashworthiness of a vehicle structure and help to improve the design by making proper investigation.

2.1.6. Implicit and Explicit analysis

Non-linear problems are solved by using either implicit or explicit analysis methods. Although both types of methods can be used to solve a non-linear problem they each have limitations. Table 2-2 shows the main difference between implicit and explicit analysis methods, which will help in selecting the best method to implement [12].

Analysis	**Implicit**	**Explicit**
Deformation	Small	Large
Event time	Long	Short
Number of Contacts	Less	Complex and large number
Material Model	Simple	Wide variety

Table 2-2, Choice criteria for implicit and explicit analysis

During crash either frontal impact or side crash total time of impact on the structure have minimum time. The deformation created by the impact is large and should be able to absorb the kinetic energy created by the impact. By referring to the above criteria table its best to use explicit analysis for conducting crashworthiness tests. In addition to the above criteria, explicit analysis allows local treatment of structural elements. This is a major advantage in identifying where the problem is and give analysis on the local section instead of changing the entire model.

2.1.7. Energy Absorption capability

Energy-absorbing is another meaning for evaluating toughness. The result is highly used in making decisions regarding the acceptance of the results obtained. Energy output encompasses multiple components, average load is identified as one of the basic determinant parameters of absorbed energy capability based on the definition of energy absorption. There are two types of energy absorption capability, specific energy absorption (SEA) and volumetric energy absorption. Specific energy absorption is defined as total energy absorbed per unit mass. Volumetric energy absorption is energy absorption per unit volume [6].

2.1.8. Safety Standards

International standards are in use in different countries to improve the structural stability of buses. The United States of America has established performance requirements for school bus roof protection according to Federal motor vehicle safety regulation No. 22 [13]. European community enforced economic commission for Europe regulation 66 concerning the approval

of large passenger vehicles concerning the strength of their super structure under dynamic rollover accident and ECE-R80 is used to specify the strength of seats and their anchorages [14]. Australian design rule (ADR 59), has specified the allowable deformation of a bus in a rollover accident. The automotive industry standard in India, AIS-031 an adopted regulation from ECE-R66 used to test crashworthiness of bus under rollover conditions. Most regulation methods are concerned with rollover accidents. However, regulations and/guidelines specifically arranged for a frontal collision of bus structure concerning the safety of driver and occupants don't exist. in the case of frontal impacts, Driver and front seat passengers are more susceptible to injuries. Protecting the driver by using a more crashworthy front frame design will ensure occupants' safety during a frontal collision. ECE-R29 is mostly imposed to ensure the safety of a truck cabin and driver during a frontal collision.

The crashworthiness requirement for a frontal collision of bus is not yet specified. The regulation for heavy truck cabin, ECE-R29, can be checked and used to improve crash characteristics of buses during a frontal collision [15]–[19]. In bus frontal collision, driver safety is related to two opposite effects: deformation of driver compartment measured by intrusion, and deceleration felt by the driver measured by amplitude and time duration of the crash pulse [16]. By using materials, which are capable of buckling in a controlled folding pattern should be used in the frontal structure to have an adequate decrease in transferred kinetic energy.

2.2. Related Works

The crashworthiness of diverse types of bus structure have been studied by many researchers [9], [13], [15], [17], [18], [20]–[22] . Numerical modeling by implementing nonlinear FE analysis is increasingly being used as an essential design and development tool by different vehicle manufacturers. Such kind computational models are replacing testing of prototypes in vehicle development, which in turn has minimized large investment efforts. Crash test methods by using FE are categorized into two, dynamic and quasi-static.

Quasi-static loading conditions are done by neglecting inertial effects. In other words, time and inertial forces will have a minor contribution to the system. This is done by applying the load so slowly that the structure deforms with minimum displacement. In the case of dynamic load, the applied load will cause the structure to vibrate and create high inertial force resulting in high deformation [4].

Pattaramon Jonpradist (2014), conducted a crashworthiness test of bus structure manufactured in Thailand under frontal impact and gave some improvements to enhance the energy absorbing capacity of the structure. The study was done based on ECE-R29 regulation. Numerical simulation was conducted by finite element modeling of bus frontal structure on Hyper mesh and analysis was performed by using explicit dynamic code ABAQUS. The result shows that the position of the steering system after impact has intruded about 125mm into driver manikin. Such kind of intrusion will injure the driver greatly causing rib bone crack and even limb bone breakage. Improving the energy absorption capacity of bus frontal design will decrease the intrusion length. The results showed that the intrusion can be reduced by up to 57% by addition energy absorbers without changing be basic structural design.

The energy-absorbing capacity of the front section of a bus during a frontal crash was investigated by Mehmet Ali [18]. The study used both Experimental and numerical methods. A nonlinear explicit finite element code LS-DYNA was used for crash analysis. And an experiment was carried out using a baseline model to check if it meets the requirement for ECE-R29. The experiment was done to validate the results found on numerical simulation and they have shown that the numerical simulation gives a valid result in regards to structural impact deformation. The energy absorbing capacity of the baseline bus model was seen week, having not to meet requirements on ECE-R29. After validating the result, the study has identified the weaker regions of the baseline body, which required reinforcement.

A study on bus rollover crashworthiness under European standard; an optimal analysis of superstructure strength using successive response was done by Cho-Chang Liang and Giang-Nam Le [14], A full scale, validated, finite element model of the bus was used. Optimization was done by using successive response surface method and parameterization of the energy absorption ability of bus frame component by using numerical simulation FE solver LS-DYNA. Bus frame optimization analysis under rollover accident was done following ECE R66 regulation. From the optimization result, it was presented that the deformation of the bus frame could be reduced by 49.2% for the lower and 39.4% for the upper side frame by only increasing the bus weight by only 1.6%. the methodology used in their study can also be implemented to study the response of different types of bus structural frames under rollover accidents.

Vivekannand Phadatare (2016), discussed the use of FEA for the improvement of crashworthiness of bus under rollover accidents. Geometric modeling of bus frames was carried out by using CAD software CATIA. Finite element modeling process by using LS-DYNA was

used for numerical simulation. There result showed that increasing the stiffness of the side structure will decrease the deformation range of the frame and prevent any part of the survival space projected outside the deformed structure. The stiffness of the bus frame is of great importance in absorbing and distributing the energy created during impact. The effective stiffness of the material and structure used will increase the crash resistance and reduce passenger injury.

Zhang Xiaoyun and Zhang Dongming (2018), a numerical simulation was made to analyze the crashworthiness of a bus during emergency braking and rollover. The study had used a multibody system for the analysis. The result showed that passengers may suffer from serious hurt during frontal crash and rollover. An improved design on the seating and side structure of the bus will reduce the injury rate.

In a study, ”crashworthiness assessment of paratransit bus” [13], numerical analysis on the structure of the modified body on chassis buses of Ford Eldorado Aerotech 240 was used. For the analysis a non-linear, explicitly, 3-D, dynamic FE code on LS-DYAN was used to simulate the crashing behavior under frontal impact and side impact with various impact velocities. the numerical result has shown that the FE model will yield tangible results and that the crashworthiness of the bus can be increased by modification and structural parts.

Side impact crashworthiness test simulation was done by Wen, et al,[22]. the super structure of a bus was tested for crashworthiness in case of a side impact. The study was done by conducting a numerical simulation on LS-DYNA. The model had consisted of the super structure of the bus and a side-impacting trolley. The side impact was done by giving the side trolley an initial velocity of 50km/hr. The final result for the displacement of the side frame was given by taking highly affected parts.

Tso-Liang Teng. et al [10], studied the application of crash pulse on the car crashworthiness design. Their study used the crash pulses obtained from frontal crash simulation of improved bumper and cross member designs for different vehicles. By implementing finite element method, the crash pulse for different models was measured in and measure head injury criterion (HIC). By comparing the results of HIC values, bumper and cross member designs with better crashworthiness were selected. The results had shown that crash pulse curves can be employed to assess the severity of occupants’ injuries.

From different literatures reviewed it was observed that, ECE-R29 mostly chosen as crashworthiness testing of bus structure in case of frontal impact by most researchers. Also, by

analyzing the crash pulse of structure in case frontal impact; HIC value can be accurately predicted the effect of crash on occupants without using a manikin. The results for HIC can be used to improve the crash response of bus structure with increased safety of occupants.

CHAPTER THREE:

3. Mathematical Modelling

3.1. Introduction

To assess the crashworthiness of any given structure it's necessary to compare the results with well-established and acceptance criteria. The numerical result of the structure under impact should be correlated with those criteria. The required quantities should be selected based on the requirement of the study at hand and by taking previously proven results regarding the structural crash tests. Different parameters have been proven to be effective in studying structural crashes by different researchers. Some and most common parameters will be implemented in the present work. The parameters to be used are Energy Absorption, Specific Energy Absorption, Peak crash force, average crash Force, crash force efficiency, crash pulse, and HIC [8].

Energy absorption (E_{abs}) is the ability of the structure of the bus to absorb the kinetic energy of the impacting body. The total kinetic energy absorbed of a given structure can be obtained by using [4]

$$E_{abs} = \int_0^{\delta} f(x)dx \qquad 3\text{-}1$$

Where, $f(x)$ is the crash force and δ is the deformation.

After finding the total energy absorbed by the structure we can determine the average crash force (F_{avg}) by dividing it by the total displacement. It's mostly recommended that this value should be maximum. Maximizing this value is mostly taken to be the best. Maintaining this high force over the deformation time shows that there are no high acceleration spikes. Average crash force can be obtained by using

$$F_{avg} = \frac{E_{abs}}{\delta} \qquad 3\text{-}2$$

The Specific energy Absorption (SE_{abs}) shows the energy absorbed per unit mass. This parameter will help in increasing our understanding of the absorption efficiency of the structure. The result can be obtained by using.

$$SEA = \frac{E_{abs}}{M} \qquad 3\text{-}3$$

The maximum force that is created during a crash will show the peak crash force. By using the value, we can determine the maximum energy that is absorbed by the structure during the crash. The peak force should occur after a long time of the crash to protect passengers from experiencing a high deceleration. Peak crash force for the structure can be represented as:

$$F_{max} = \max(f_x) \quad 3\text{-}4$$

Now by dividing the average crash force by peak crash force we will find the crash force efficiency (CFE) of the structure.

$$CFE = \frac{F_{avg}}{F_{max}} \quad 3\text{-}5$$

A CFE value close or equal to 1 shows that the deformation of a given structure is steady and the crashing force applied is almost the same trough out the deformation process, which is unlikely to occur in structure crash response. A value close to 0 shows a high peak value at the initial stage of the crash. This will decrease the ability of the structure to absorb the crash energy. A structure with a better CFE minimizes the force spikes in the crash, leading to fewer accelerations in the structure and better safety [23].

In addition to the above parameters, the Head injury criterion (HIC) number is used to assess the crashworthiness of the structure. HIC number indicates the likelihood of head injury to occur due to the movement of the head [11], [10] [24]. The value for HIC for a given crash pulse within a given period can be found by using the following equation.

Where, a (t) is resultant acceleration, in g (gravitational acceleration)

$$HIC = Max\left[\frac{1}{t_2 - t_1}\int_{t_1}^{t_2} a(t)dt\right]^{2.5}(t_2 - t_1) \quad 3\text{-}6$$

t_1 and t_2 represent the initial and final instant of time travel respectively and $t_2 - t_1 \leq 36\ ms$

HIC value of 1000 represents the “safe” limit of human tolerance, above this value, the risk of a severe head injury may occur. The crash pulse curve found from the frontal impact of the structure can be employed to assess the severity of occupants’ injuries [24].

3.2. Basic of inelastic impact

During impact, the load is transferred between two bodies in a fraction of a second. During impact, energy is transferred between the colliding bodies. Due to non-linearity and material property, some of the colliding entities' energy transferred will be absorbed inside the frame resulting in deformation, crack, or other modes of failure. The amount of energy transferred should be analysed to find the energy absorbing capacity of the colliding body. The concepts in the conservation of linear momentum and conservation of energy can be used to find the total energy transferred [3].

As illustrated in the figure below, taking a stationary mass M1 being struck by a mass M2 traveling at a velocity of V_2.

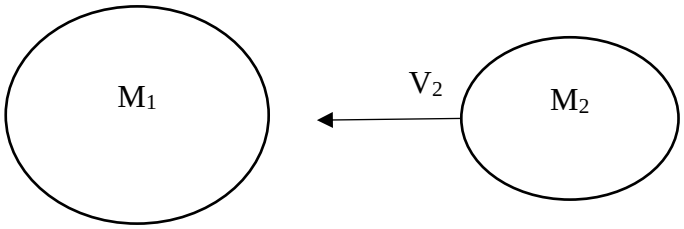

Figure 3-1, in elastic impact model

Where: M_1 Mass of mass 1

M_2 Mass of mass 2

V_2 initial velocity of mass 2

Conservation of linear momentum just after impact

$$M_2V_2 = (M_1 + M_2)V_3 \qquad 3\text{-}7$$

In equation 1 the common velocity of the masses just after inelastic impact is represented by V_3. Know taking conservation of energy and assuming that there is no transfer or loss of energy during impact. The energy balance equation before and after impact is expressed as follows.

$$M_2\frac{V_2^2}{2} = (M_1 + M_2)\frac{V_3^2}{2} \qquad 3\text{-}8$$

For perfectly elastic collision equation 3-8 shows that the energy is conserved before and after impact. In an inelastic impact, there is a loss in kinetic energy during impact. The total energy loss during impact will be absorbed by the two bodies. The net kinetic energy loss during impact is

$$K_L = M_2 \frac{V_2^2}{2} - (M_1 + M_2) \frac{V_3^2}{2} \quad 3\text{-}9$$

Taking the value of V_3 from equation 1 and simplifying equation 3 will yield

$$K_L = M_2 \frac{V_2^2}{2} / (1 + \frac{M_2}{M_1}) \quad 3\text{-}10$$

Equation 3-9 gives the energy which must be absorbed by the two masses. The same procedure can be used to find the energy loss/transfer during impact for both masses having initial velocity. Finding the net energy transfer will help in analyzing the energy absorbing capacity of the structure bus.

The total energy absorbed per unit mass of impacting material can be defined by using specific energy absorption. First, the total energy absorbed in a single impacting mass can be expressed as

$$E = \int_a^b P dx \quad 3\text{-}11$$

Where E energy absorbed in impacting mass

P means crash load

a & b are total crash distances starting from initial contact to separation

now the specific energy per unit mass is given as

$$E_s = \frac{E}{m} = \frac{\int_a^b P dx}{m} \quad 3\text{-}12$$

3.3. Nonlinear Finite element analysis

Nonlinear finite element method is used to find the solution of a system where the most required parameters are strength analysis, stability analysis, service configuration, and progressive failure analysis (crash, crack. Buckling, and the like). Sources for nonlinear in finite element analysis are classified into three main categories.

a. **Material nonlinearity**: - in this case material response depends on the current deformation and possibly past deformation history.
b. **Geometric nonlinearity: -** Geometrical non-linearity of the system is taken into consideration.

c. **Boundary condition nonlinearity**: - Applied force or displacement depends on the deformation of the structure.

Bus structural frame consists of different components with dissimilar geometry. During impact, most components experience high stress, once the applied stress passes yield load/ buckling limit the structural parts undergo elastic-plastic deformation. This occurs in a short period. Solving the system in a direct approach is complex and will result in errors. Implementing numerical solutions will give a precise solution.

In the crashing process of a public bus, the crashing phenomena will result in the material property (like Stiffness) and Geometrical property (like Shape) of the structure changing with time. Accordingly, using nonlinear finite element approach is best suited to find the required outcome. As discussed in the literature review there are different commercial software's to conduct numerical analysis. Amongst one of the common numerical software used to solve nonlinear finite element equations concerning structural crash ABAQUS.

In this section, the theoretical background of the procedure for nonlinear finite element analysis will be discussed and numerical simulation of some of the basic sections of the bus structural parts is covered. Finally, crashworthiness of the structure in case of frontal and side-impact by using numerical analysis will be done by following internationally known and accepted procedures.

3.3.1. Governing Equation

ABAQUS is capable of simulating brief transient dynamic events like crashworthiness. The governing equation for nonlinear finite element analysis of a given system is based on the principle of virtual power [20]. The main finite element equation can be solved by using

$$[M]\{\ddot{U}\} + [C]\{\dot{U}\} + [K]\{U\} = \{F(t)\} \qquad 3\text{-}13$$

Where, $[M]$, Global mass matrix

$\{\ddot{U}\}, \{\dot{U}\}, \{U\}$, Nodal acceleration, velocity, and displacement

$[C]$, Global damping coefficient

$[K]$, Stiffness matric

$F(t)$, Applied external load

Here it should be noted that for a problem with material and geometry non-linearity as in crashworthiness problems, the stiffness matric $[K]$ and damping matric $[C]$ are not constant. Instead, they are a function of displacement and consequently of time as well. the solution for the nodal acceleration.

$$\{\ddot{U}\} = [M]^{-1}.[\{F(t)\} - \{[C]\{\dot{U}\} + [K]\{U\}\}] \quad 3\text{-}14$$

Taking equation 3-3 for a single element the general equation can be represented as

$$[m]\{\ddot{u}\} + [c]\{\dot{u}\} + [k]\{u\} = \{f(t)\} \quad 3\text{-}15$$

Where m, *u* , *k,* and *f(t)* are mass, displacement, stiffness, and force on a given element

Direct solving of the above equation is difficult and time-consuming. Instead, an approximate general solution can be given. The approximated solution for displacement can be expressed as a sum of several functions that are called trail function/shape function/interpolation function. In finite element method the motion $u_i(x)$ is approximated as.

$$u_i(x) = \sum_{i=1}^{n} d_e N_i \quad 3\text{-}16$$

Where n = number of terms

$N_i(x)$ = Trial/shape function

d_e = coefficient to be determined by minimizing

The trial function and coefficients are chosen so that the general solution satisfies the boundary condition of the given problem.

There are different types of finite elements that can be used. The selection of which type depends on the domain that needs to be discretized and the order of the trial function that is used to find the approximate solution. For three body a tetrahedral element is best suited to have a valid result for crash simulation. Taking a linear tetrahedral element

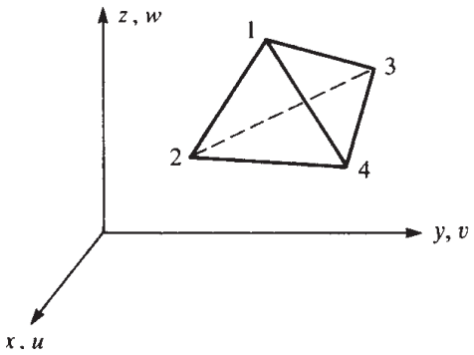

Figure 3-2, Linear tetrahedral element

For an element represented in Figure 3-2, nodal displacement can be represented as,

$$\{d\} = \begin{Bmatrix} u_1 \\ v_1 \\ w_1 \\ u_2 \\ v_2 \\ w_2 \\ u_3 \\ v_3 \\ w_3 \\ u_4 \\ v_4 \\ w_4 \end{Bmatrix} \qquad 3\text{-}17$$

For a liner tetrahedral element, we can use a linear function to resent the general displacement function for each corner node.

$$u(x, y, x) = a_1 + a_2 x + a_3 y + a_4 z$$

$$v(x, y, x) = a_5 + a_6 x + a_7 y + a_8 z$$

$$w(x, y, x) = a_9 + a_{10} x + a_{11} y + a_{12} z$$

The matrix shape function at each node has the form

$$N = \begin{bmatrix} N_1 & 0 & 0 & N_2 & 0 & 0 & N_3 & 0 & 0 & N_4 & 0 & 0 \\ 0 & N_1 & 0 & 0 & N_2 & 0 & 0 & N_3 & 0 & 0 & N_4 & 0 \\ 0 & 0 & N_1 & 0 & 0 & N_2 & 0 & 0 & N_3 & 0 & 0 & N_4 \end{bmatrix} \qquad 3\text{-}18$$

By using volume coordinate, we can develop the shape function. Using volume coordinate is more convenient for developing shape function construction and element matric integration. By using this method, the general displacement functions can be obtained as follows.

$$u(x,y,z) = \frac{1}{6V}\{(\propto_1 + \beta_1 x + \gamma_1 y + \delta_1 z)u_1 + (\propto_2 + \beta_2 x + \gamma_2 y + \delta_2 z)u_2 + (\propto_3 + \beta_3 x + \gamma_3 y + \delta_3 z)u_3 + (\propto_4 + \beta_4 x + \gamma_4 y + \delta_4 z)u_4\}$$

$$v(x,y,z) = \frac{1}{6V}\{(\propto_1 + \beta_1 x + \gamma_1 y + \delta_1 z)v_1 + (\propto_2 + \beta_2 x + \gamma_2 y + \delta_2 z)v_2 + (\propto_3 + \beta_3 x + \gamma_3 y + \delta_3 z)v_3 + (\propto_4 + \beta_4 x + \gamma_4 y + \delta_4 z)v_4\} \quad 3\text{-}19$$

$$w(x,y,z) = \frac{1}{6V}\{(\propto_1 + \beta_1 x + \gamma_1 y + \delta_1 z)w_1 + (\propto_2 + \beta_2 x + \gamma_2 y + \delta_2 z)w_2 + (\propto_3 + \beta_3 x + \gamma_3 y + \delta_3 z)w_3 + (\propto_4 + \beta_4 x + \gamma_4 y + \delta_4 z)w_4\}$$

Where, 6V is the volume of the tetrahedron and can be found by evaluating the determinant

$$6V = \begin{vmatrix} 1 & x_1 & y_1 & z_1 \\ 1 & x_2 & y_2 & z_2 \\ 1 & x_3 & y_3 & z_3 \\ 1 & x_4 & y_4 & z_4 \end{vmatrix} \quad 3\text{-}20$$

Now the coefficients α, β, γ are the cofactors of the above determinant matrix, which can be represents

$$\alpha_1 = \begin{vmatrix} x_2 & y_2 & z_2 \\ x_3 & y_3 & z_3 \\ x_4 & y_4 & z_4 \end{vmatrix} \beta_1 = \begin{vmatrix} 1 & y_2 & z_2 \\ 1 & y_3 & z_3 \\ 1 & y_4 & z_4 \end{vmatrix} \gamma_1 = \begin{vmatrix} 1 & x_2 & z_2 \\ 1 & x_3 & z_3 \\ 1 & x_4 & z_4 \end{vmatrix} \delta_1 = \begin{vmatrix} 1 & x_2 & y_2 \\ 1 & x_3 & y_3 \\ 1 & x_4 & y_4 \end{vmatrix} \quad 3\text{-}21$$

$$\alpha_2 = \begin{vmatrix} x_1 & y_1 & z_1 \\ x_3 & y_3 & z_3 \\ x_4 & y_4 & z_4 \end{vmatrix} \beta_2 = \begin{vmatrix} 1 & y_1 & z_1 \\ 1 & y_3 & z_3 \\ 1 & y_4 & z_4 \end{vmatrix} \gamma_2 = \begin{vmatrix} 1 & x_1 & z_1 \\ 1 & x_3 & z_3 \\ 1 & x_4 & z_4 \end{vmatrix} \delta_2 = \begin{vmatrix} 1 & x_1 & y_1 \\ 1 & x_3 & y_3 \\ 1 & x_4 & y_4 \end{vmatrix} \quad 3\text{-}22$$

$$\alpha_3 = \begin{vmatrix} x_1 & y_1 & z_1 \\ x_2 & y_2 & z_2 \\ x_4 & y_4 & z_4 \end{vmatrix} \beta_3 = \begin{vmatrix} 1 & y_1 & z_1 \\ 1 & y_2 & z_2 \\ 1 & y_4 & z_4 \end{vmatrix} \gamma_3 = \begin{vmatrix} 1 & x_1 & z_1 \\ 1 & x_2 & z_2 \\ 1 & x_4 & z_4 \end{vmatrix} \delta_3 = \begin{vmatrix} 1 & x_1 & y_1 \\ 1 & x_2 & y_2 \\ 1 & x_4 & y_4 \end{vmatrix} \quad 3\text{-}23$$

$$\alpha_4 = \begin{vmatrix} x_1 & y_1 & z_1 \\ x_2 & y_2 & z_2 \\ x_3 & y_3 & z_3 \end{vmatrix} \beta_4 = \begin{vmatrix} 1 & y_1 & z_1 \\ 1 & y_2 & z_2 \\ 1 & y_3 & z_3 \end{vmatrix} \gamma_4 = \begin{vmatrix} 1 & x_1 & z_1 \\ 1 & x_2 & z_2 \\ 1 & x_3 & z_3 \end{vmatrix} \delta_4 = \begin{vmatrix} 1 & x_1 & y_1 \\ 1 & x_2 & y_2 \\ 1 & x_3 & y_3 \end{vmatrix} \quad 3\text{-}24$$

The general displacement equation given on equation 3-16 can be equivalently expressed in terms of shape function and nodal displacement equation

$$\begin{Bmatrix} u \\ v \\ w \end{Bmatrix} = \begin{bmatrix} N_1 & 0 & 0 & N_2 & 0 & 0 & N_3 & 0 & 0 & N_4 & 0 & 0 \\ 0 & N_1 & 0 & 0 & N_2 & 0 & 0 & N_3 & 0 & 0 & N_4 & 0 \\ 0 & 0 & N_1 & 0 & 0 & N_2 & 0 & 0 & N_3 & 0 & 0 & N_4 \end{bmatrix} \begin{Bmatrix} u_1 \\ v_1 \\ w_1 \\ u_2 \\ v_2 \\ w_2 \\ u_3 \\ v_3 \\ w_3 \\ u_4 \\ v_4 \\ w_4 \end{Bmatrix} \quad 3\text{-}25$$

Where the shape functions are given by,

$$N_1 = \frac{\alpha_1 + \beta_1 x + \gamma_1 y + \delta_1 z}{6V} \qquad N_2 = \frac{\alpha_2 + \beta_2 x + \gamma_2 y + \delta_2 z}{6V}$$

$$N_3 = \frac{\alpha_3 + \beta_3 x + \gamma_3 y + \delta_3 z}{6V} \qquad N_4 = \frac{\alpha_4 + \beta_4 x + \gamma_4 y + \delta_4 z}{6V} \quad 3\text{-}26$$

Element strains for a three-dimensional stress state is given by

$$\{\varepsilon\} = \begin{Bmatrix} \varepsilon_x \\ \varepsilon_y \\ \varepsilon_z \\ \gamma_{xy} \\ \gamma_{yz} \\ \gamma_{zx} \end{Bmatrix} = \begin{Bmatrix} \frac{\partial u}{\partial x} \\ \frac{\partial v}{\partial y} \\ \frac{\partial w}{\partial z} \\ \frac{\partial u}{\partial y} + \frac{\partial v}{\partial x} \\ \frac{\partial v}{\partial z} + \frac{\partial w}{\partial y} \\ \frac{\partial w}{\partial x} + \frac{\partial u}{\partial z} \end{Bmatrix} \text{-} \quad 3\text{-}27$$

With

$$\frac{\partial u}{\partial x} = \frac{\partial}{\partial x}(N_1 u_1 + N_2 u_2 + N_3 u_3 + N_4 u_4)$$

$$\frac{\partial v}{\partial y} = \frac{\partial}{\partial y}(N_1 v_1 + N_2 v_2 + N_3 v_3 + N_4 v_4) \quad 3\text{-}28$$

$$\frac{\partial w}{\partial z} = \frac{\partial}{\partial w}(N_1 w_1 + N_2 w_2 + N_3 w_3 + N_4 w_4)$$

By simplifying partial differential equations, the values of derivatives will be

$$\frac{\partial u}{\partial x} = \frac{1}{6V}(\beta_1 u_1 + \beta_2 u_2 + \beta_3 u_3 + \beta_4 u_4)$$

$$\frac{\partial v}{\partial y} = \frac{1}{6V}(\gamma_1 v_1 + \gamma_2 v_2 + \gamma_3 v_3 + \gamma_4 v_4)$$

$$\frac{\partial w}{\partial z} = \frac{1}{6V}(\delta_1 w_1 + \delta_2 w_2 + \delta_3 w_3 + \delta_4 w_4)$$

$$\frac{\partial u}{\partial y} + \frac{\partial v}{\partial x} = \frac{1}{6V}(\gamma_1 u_1 + \gamma_2 u_2 + \gamma_3 u_3 + \gamma_4 u_4 + \beta_1 v_1 + \beta_2 v_2 + \beta_3 v_3 + \beta_4 v_4) \quad \text{3-29}$$

$$\frac{\partial v}{\partial z} + \frac{\partial w}{\partial y} = \frac{1}{6V}(\delta_1 v_1 + \delta_2 v_2 + \delta_3 v_3 + \delta_4 v_4 + \gamma_1 w_1 + \gamma_2 w_2 + \gamma_3 w_3 + \gamma_4 w_4)$$

$$\frac{\partial w}{\partial x} + \frac{\partial u}{\partial z} = \frac{1}{6V}(\beta_1 w_1 + \beta_2 w_2 + \beta_3 w_3 + \beta_4 w_4 + \delta_1 u_1 + \delta_2 u_2 + \delta_3 u_3 + \delta_4 u_4)$$

Substituting equation 3-29 into equation 3-27 will give strain equation in a three-dimensional element

$$\{\varepsilon\} = \begin{Bmatrix} \varepsilon_x \\ \varepsilon_y \\ \varepsilon_z \\ \gamma_{xy} \\ \gamma_{yz} \\ \gamma_{zx} \end{Bmatrix}$$

$$= \frac{1}{6V}\begin{Bmatrix} \beta_1 & 0 & 0 & \beta_2 & 0 & 0 & \beta_3 & 0 & 0 & \beta_4 & 0 & 0 \\ 0 & \gamma_1 & 0 & 0 & \gamma_2 & 0 & 0 & \gamma_3 & 0 & 0 & \gamma_4 & 0 \\ 0 & 0 & \delta_1 & 0 & 0 & \delta_2 & 0 & 0 & \delta_3 & 0 & 0 & \delta_4 \\ \gamma_1 & \beta_1 & 0 & \gamma_2 & \beta_2 & 0 & \gamma_3 & \beta_3 & 0 & \gamma_4 & \beta_4 & 0 \\ 0 & \delta_1 & \gamma_1 & 0 & \delta_2 & \gamma_2 & 0 & \delta_3 & \gamma_3 & 0 & \delta_4 & \gamma_4 \\ \delta_1 & 0 & \beta_1 & \delta_2 & 0 & \beta_2 & \delta_3 & 0 & \beta_3 & \delta_4 & 0 & \beta_4 \end{Bmatrix} \begin{Bmatrix} u_1 \\ v_1 \\ w_1 \\ u_2 \\ v_2 \\ w_2 \\ u_3 \\ v_3 \\ w_3 \\ u_4 \\ v_4 \\ w_4 \end{Bmatrix} \quad \text{3-30}$$

Simplifying the above matrix equation can be represented as

$$\{\varepsilon\} = [B]\{d\} \tag{3-31}$$

For a constitutive relationship for plane stress/plane strain elements, the stress and strain relationships are represented by

$$\begin{Bmatrix} \sigma_x \\ \sigma_y \\ \sigma_z \\ \tau_{xy} \\ \tau_{yz} \\ \tau_{zx} \end{Bmatrix} = [D] \begin{Bmatrix} \varepsilon_x \\ \varepsilon_y \\ \varepsilon_z \\ \gamma_{xy} \\ \gamma_{yz} \\ \gamma_{zx} \end{Bmatrix} \tag{3-32}$$

$$[D] = \frac{E}{(1+v)(1-2v)} \begin{bmatrix} 1-v & v & v & 0 & 0 & 0 \\ v & 1-v & v & 0 & 0 & 0 \\ v & v & 1-v & 0 & 0 & 0 \\ 0 & 0 & 0 & \frac{1-2v}{2} & 0 & 0 \\ 0 & 0 & 0 & 0 & \frac{1-2v}{2} & 0 \\ 0 & 0 & 0 & 0 & 0 & \frac{1-2v}{2} \end{bmatrix} \tag{3-33}$$

After finding the value for all the variables required, the stiffness matric for a tetrahedral element can be found by using,

$$[k] = [B]^T [D]^T [B] V \tag{3-34}$$

3.3.2. Explicit nonlinear finite element analysis

From equations 3-1 and 3-2 it was shown that the second-order differential equation. The equation of motion should be stratified at each time step,

$$M\ddot{u}^n = f^n \tag{3-35}$$

$$f^n = f_{ext}^n - f_{int}^n \tag{3-36}$$

For a given time step n, equation 3-6 is integrated in time. To do so the central difference method is used in the ABAQUS program. The central difference method is among the most common of the explicit methods used to solve finite element equations. The time step solution for the nonlinear equation is solved by following the procedure described below [2].

Step 1. Initial conditions: to solve the second-order nonlinear differential equation, it requires two initial conditions the displacement $u(0)$ and velocity $\dot{u}(0)$ at time $t = 0$. Also initial values of other material state variables and compute mass (M).

Step 2. Loop over each element and solve force.

$$u_e^{n+1} = L_e u^{n+1} \quad (3\text{-}37)$$

$$\varepsilon_e^{n+1} = B_e u_e^{n+1} \quad (3\text{-}38)$$

$$\sigma_e^{n+1} = \sigma_e^n + \Delta\sigma_e = f(\varepsilon_e^n, \varepsilon_e^{n+1}) \quad (3\text{-}39)$$

$$f_{int,e}^{n+1} = \int_{\Omega_e} B_e^T \sigma_e^{n+1} d\Omega \quad (3\text{-}40)$$

Step 3. Assemble the force equation

$$f_{int}^{n+1} = \sum_e L_e^T f_{int,e}^{n+1} \quad (3\text{-}41)$$

$$f_{ext}^{n+1} = \sum_e L_e^T f_{ext,e}^{n+1} \quad (3\text{-}42)$$

$$\sigma_e^{n+1} = \sigma_e^n + \Delta\sigma_e = f(\varepsilon_e^n, \varepsilon_e^{n+1}) \quad (3\text{-}43)$$

$$f^{n+1} = f_{ext}^{n+1} - f_{int}^{n+1} \quad (3\text{-}44)$$

Step 4. Compute new acceleration

$$\ddot{u}^{n+1} = M^{-1} f^{n+1} \quad (3\text{-}45)$$

Step 5. Time update

$$t^{n+1} = t^n + t^{n+\frac{1}{2}}, t^{n+\frac{1}{2}} = \frac{1}{2}(t^n + t^{n+1}) \quad (3\text{-}46)$$

Step 6. find the new partial update nodal velocity and check energy balance at time step n.

$$\dot{u}^{n+\frac{3}{2}} = \dot{u}^{n+1/2} + \Delta t \ddot{u}^{n+1} \quad (3\text{-}47)$$

Step 7. Update the nodal displacement

$$u^{n+1} = u^n + \Delta t \dot{u}^{n+1/2} \quad 3\text{-}48$$

after the final step analysis will repeat the process starting from step 2. And will loop until all nodes in each element are covered.

Where, $M =$ mass matrix

$n =$ number of time steps

t = time

$u^n, \dot{u}^n, \ddot{u}^n$ = nodal displacement, velocity, and acceleration at time $t = n\Delta t$

$f^n, f_{ext}^n, f_{int}^n$ = resultant, external and internal nodal forces at time $t = n\Delta t$

$\varepsilon_e^n, \sigma_e^n$ = strain and stress tensors of an element at time $t = n\Delta t$

B_e^T = Strain-displacement matrix of element

L_e^T = Boolean connectivity matrix of an element.

Explicit time discretization method requires a time step smaller than a critical value Δt_{cr}. If the time step is greater than the critical time step, the solution of the equation is artificially amplified during the step-by-step procedure, due to the accumulation of the discretization error. If the system does not have damping, the critical time step can be simplified to

$$\Delta t_{cr} = 2/\omega_{max} \quad 3\text{-}49$$

Where, ω_{max} the highest angular frequency in the system

For a discrete system, the time step must be small enough to excite all frequencies in the finite element mesh. This requires such a short time step that the shock wave does not miss any node when traveling the mesh.

$$\Delta t \leq l_{cr}/c \quad 3\text{-}50$$

Where, l_{cr} critical length of the element

Elements, nodes, and even other components like springs or contact time steps can be calculated and the global time step can be adjusted for a maximum value that makes the computation time as small as possible without compromising the results with error introduction. Accordingly, the time-step is given by,

$$\Delta t_{cr} = \frac{l}{c} = \frac{l}{\sqrt{\frac{E}{\gamma}}} \quad 3\text{-}51$$

After finding critical time step the natural frequency of can be shown by using the following equation [25].

$$f = \frac{\omega}{2\pi} \qquad 3\text{-}52$$

Where: ω is angular frequency, and can be found by using equation 3-49

While discretizing the element size should be selected properly. If the selected size is large the model will have low precision and if the element is too small it will produce a low time step and large computational time.

The most suitable method to analyze the crashworthiness of a structure is dynamic analysis. To validate the selected model experimental data is more required but it's more difficult to obtain. Such kind of experiment is expensive and not reachable in this research. Adapting the dynamic FEA explicit analysis, a more economical and reliable result of what would happen in an impact test can be obtained and the structure can be sized to accomplish the project goals. This way it is possible to have an idea of the performance and crashworthiness of the studied structure when implemented in the partial and full model subjected to frontal and side-impact.

3.4. Crashworthiness testing methods

3.4.1. Frontal crash test method

For the current study full-frontal crash and offset frontal crash are considered for analyzing the crashworthiness of the structure under different crash conditions. For full-frontal impact testing parameters in ECE-R29 regulation were used. In offset frontal impact test was done by using a fixed rigid wall and applying velocity to complete structure, initial velocity to the structure was set at 48 km/hr (13.33 m/s) as stated in U.S- FMVSS/208 regulation [16].

The frontal impact test is done following ECE-R29, the regulation involves an impacting pendulum test in which the safety of a truck cabin and drivers. Regulation specifically arranged for bus in case of frontal crash does not exist [17], Most scholars and crash test facilities use this regulation to check crashworthiness of buses under frontal impact. For vehicles with gross vehicle mass exceeding 7.5 tons, the pendulum impact energy of 55kJ must be applied [26]. Figure 3-3**.** show the general arrangement and dimension of the test method. The impactor plate is made up of steel material and has a mass of 1,500Kg. It has a rectangular shape with a width of 2,500 mm and height of 800 mm and should be suspended 3,500 mm up from the geometric center of the impactor. The position of the pendulum plate should be arranged in vertical

distance between the center of gravity of the pendulum plate and the R-point of the driver's seat is 50 mm.

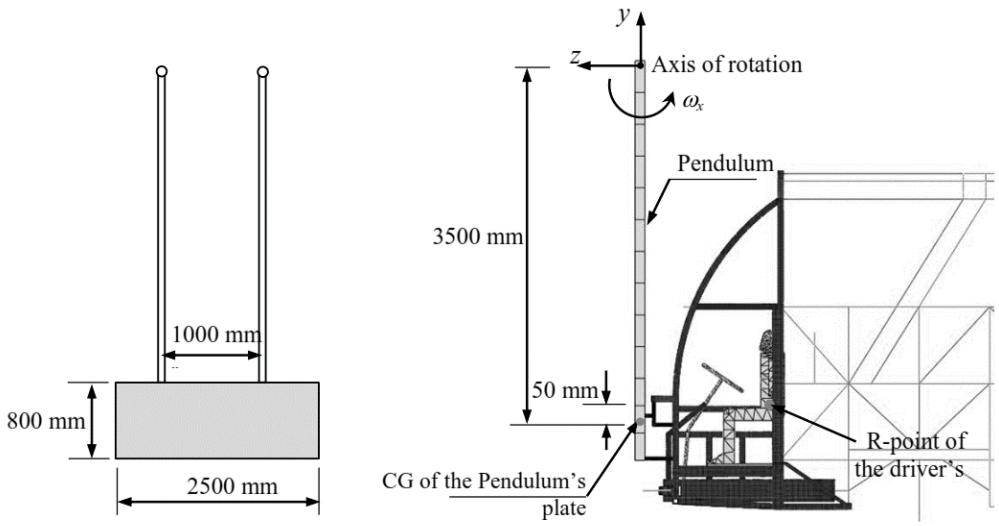

Figure 3-3, Frontal impact test according to ECE-R29 [23]

According to ECE-R29 regulation, the impact energy is given to the bus structure in form of kinetic energy. The required Impact angular velocity (ω), can be calculated by applied impact energy E, as

$$E = \frac{1}{2} I_{xx} \omega_x^2 \qquad 3\text{-}54$$

$$I_{xx} = I_{xc} + mL^2 \qquad 3\text{-}55$$

Under these conditions, the driver's survival space should be checked after the test. To achieve this properly sized manikin should be used, which is described in the regulation. The fiftieth-percentile male body manikin is shown in Figure 3-4. The dimensions for manikin are based on ECE-R29 recommendations. After modeling, finite element analysis of the study is done by using explicit nonlinear element code in ABAQUS. To meet the requirements, there should not be any contact between manikin and front structure member or steering wheel after the impact. The bus body for the analysis will consist of the front structure, right and left side walls, roof and steering system.

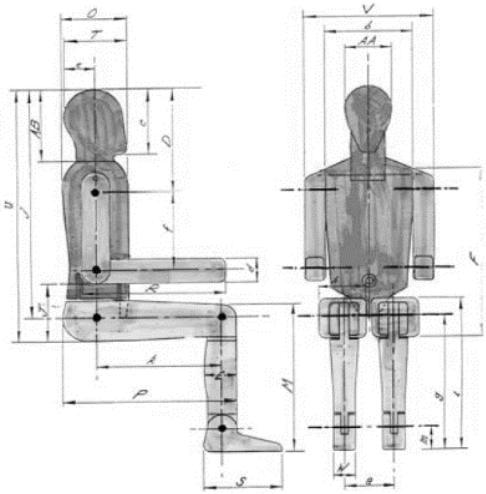

Figure 3-4, Fiftieth-percentile male body manikin used in ECE-R29 [17]

In addition to the frontal crash test as per ECE-R29, an offset impact test with a rigid wall is done to check the crashworthiness of the structure in such cases of accidents. Testing the structure's response in case of different impact conditions will give a better understanding of the crashworthiness of the structure. The test is arranged to simulate a bus crashing into a wall (rigid wall). Initial velocity of structure is set to 56 km/hr (15.55 m/s) [16]. The simulation results are used to identify the response of the structure to such kinds of impacts and identify critical structure areas, which are exposed to severe structural damage.

3.4.2. Side crash Test Method

There are few works of literature and journals done on the side impact of buses. As in frontal impact, there are no specific regulations in regards to structural response in the case of a side impact of buses. Some researchers use the residual space articulated on ECE R-66 regulation, which is mainly used for roll-over test, and side ECE R-95 side impact regulation for Automobiles. Residual space as defined in ECE R-66 regulation residual space is defined as “A space to be preserved in the passengers, crew and driver’s compartment(s) to provide better survival possibility for passengers, driver, and crew in case of a rollover accident.” By using the same residual space, we check the crashing behavior of the side and floor members of the bus structure. Some researchers [23] [20] , have used the same procedure to study the crashing behavior of buses in case of a side impact.

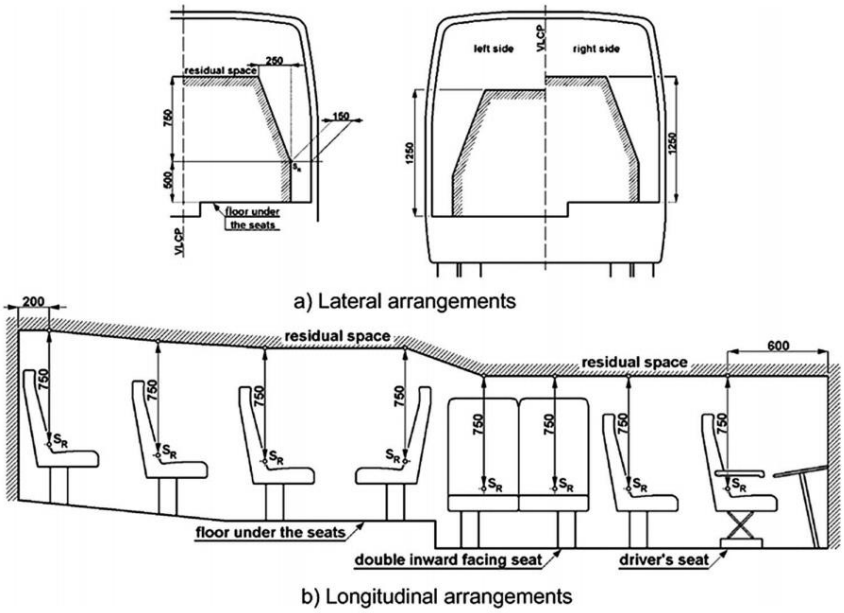

Figure 3-5, Residual space measured in millimeters, ECE R66 (a) front view (b) side view [4]

As shown in figure 3-5, the space between side structure and residual space is taken to be 150 mm. if the side structure during and after impact reaches or passes this limit injury to passengers will be severe. A side impactor trolley will collide with the side structure of the bus with a speed of 48km/hr [23][13]. Side impact crashworthiness is tested in two different scenarios, one is side perpendicular impact and side angled impact. for side angled impact the trolley is positioned 27º of its initial position. Figure 3-6 shows the general arrangement of the side impact test for both scenarios.

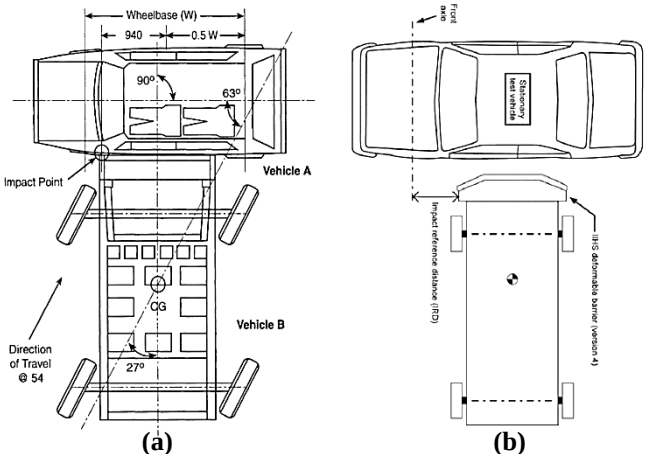

Figure 3-6, Side impact arrangements (a) for side angled impact (b) side perpendicular

CHAPTER FOUR:

4. Finite element modeling

For this study, a commercial software ABAQUS is used to conduct numerical analysis. As discussed earlier the simulation is done by following standards and regulations proposed on ECE-R29 and adoption of ECE-R60. In this section numerical analysis is done to determine the crashworthiness of the structure. The final results targeted to show the crashing behavior of the bus in terms of parameters discussed in chapter three.

Development of the finite element model for crashworthiness testing follows CAD modeling, Preprocessing, Analysis, and postprocessing. As the structure has a complex shape to model it all in ABAQUS, a three-dimensional geometrical model of the structure was made by using CATIA, and the required component for each simulation was imported for finite element analysis to ABAQUS.

4.1. Geometrical modeling

The 3D model of the bus structure was developed by using CATIA V5 software. The total geomatical data were collected by conducting a field study and direct measurement on 60-seated bus structure frames being manufactured. Different steel bars geometries were used to construct the structure of the bus. Most commonly used are rectangular thin-walled tubes having different grades for each section of the structure. Side and rear structural frames were developed from RHS (70×50×2.5) mm and (50×30×2.5) mm. The roof structure was constructed from RHS (40×40×2.5) mm. Whereas the floor cross members are mainly constructed from a C-channel bar with (80×40×4) mm. The material property of the materials used was taken from standards and is seen all to be made out of mild steel having the following properties elastic properties.

Material Property	Value
Density	7850 kg/m3
Modulus of elasticity E	210 Gpa
Shear modulus	810 Gpa
Yield strength	235 Mpa
Ultimate strength	360 Mpa
Poisson's ratio	0.3

Table 4-1, Material Property [27]

Since the structure undergoes high deformation in the plastic range. The plastic properties of material should be defined. For the current study, the Johnson-cook strength model is used to define the stress-strain relationship. Table 4-2 shows the J-C strength model constants for mild steel.

A(MPa)	B(MPa)	n	C
217	233.7	0.6428	0.0756

Table 4-2, J-C strength model constants for mild steel [28]

A summary of the dimensions and shape of materials used for constructing the bus frame is shown in Figure 4-1. The dimensions are taken by direct measurement from local bus body builders.

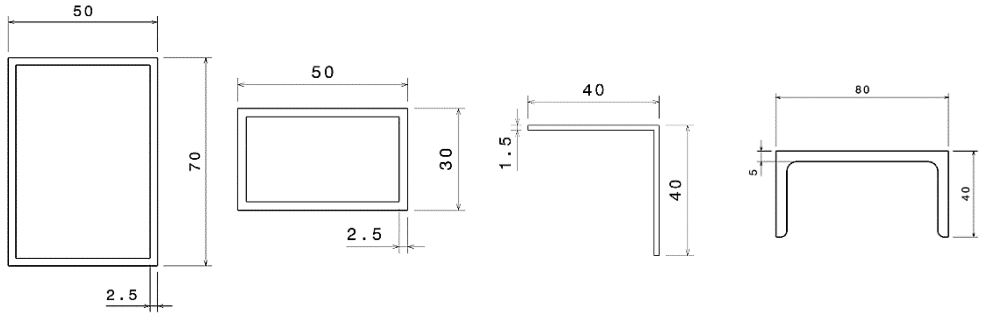

Figure 4-1, Cross sectional area of materials most commonly used in the structure (*all dimensions are in mm*)

After collecting the necessary dimensions and materials the 3D Geometrical model of the bus structural frame was developed by using CATIA V5R19.

The main geometrical models of all the parts of the structure were only considered for evaluating the crashing behavior in the case of frontal impact and side-impact testing. The bus has a height of 2.8 m (from the ground), width 2.4 m, and length of 12 m. The total weight of the structure is estimated to be 1,800 kg. The geometrical model of the structure is as shown in Figures 4-2.

After completing the geometrical modeling of the structure, the required section of the model for frontal and side-impact crashworthiness tests was imported into ABAQUS CAE module.

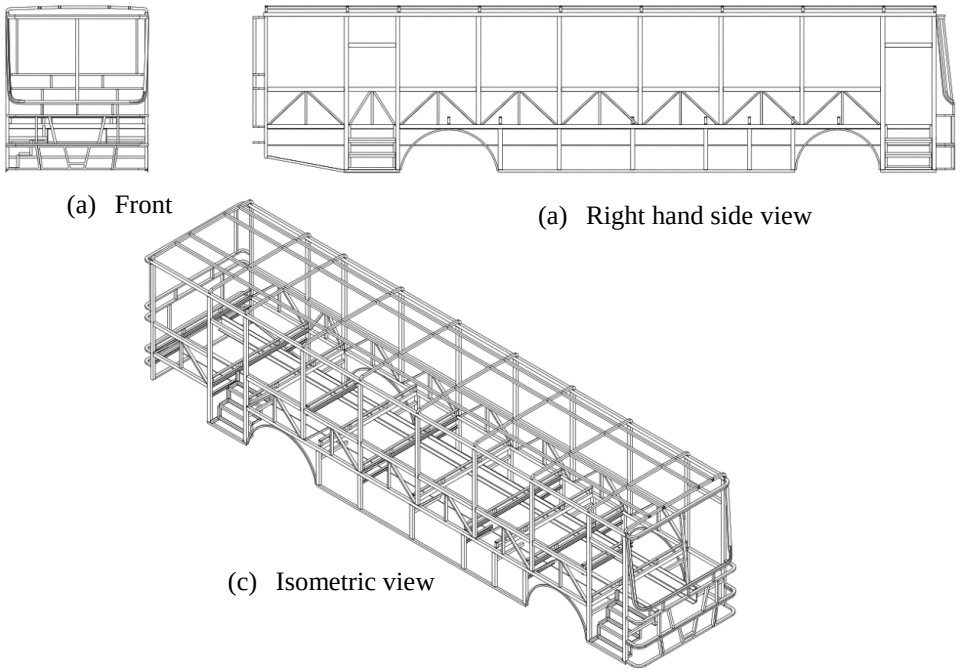

(a) Front

(a) Right hand side view

(c) Isometric view

Figure 4-2, Front, side, and isometric drawing of bus structure

4.2. Simulation setup

There are various types of standard crash simulation methods that are being used for studying the crashworthiness of vehicles [6] [25] [14] [27]. As discussed in chapter three the main regulations implemented are ECE-R29 and adopted residual space from ECE-R60 for frontal and side crashes respectively. In addition to the two main benchmarks, additional simulations for a frontal-offset crash were implemented for testing the crashworthiness of the structure.

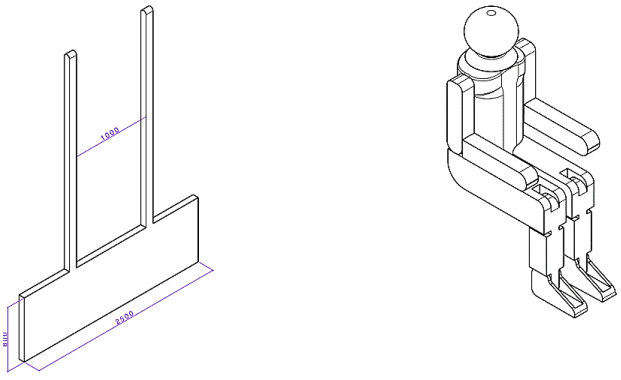

(b) Impactor model

(c) Manikin model

Figure 4-3, Impactor plate and manikin to be used for frontal impact

The Frontal bus structure will be crashed by the pendulum as described in the regulation. To meet the requirements, there should not be any contact between manikin and front structure member or steering wheel during and after the impact. As described in the regulation the bus body required for the analysis consists of the front structural frame, right and left sidewalls, roof, and steering wheel model. The general arrangement of the model to be used for the simulation is as shown in the figure below.

For side crash testing, residual space described on ECE-R60 will be used to check the structure's deformation method. When the side structure is hit with a trolley the deformed frame should not intrude into residual space. Figure 4-5 shows the full structure with residual space assigned.

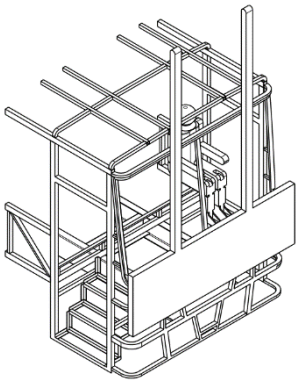

Figure 4-4, Front structure model for front impact test

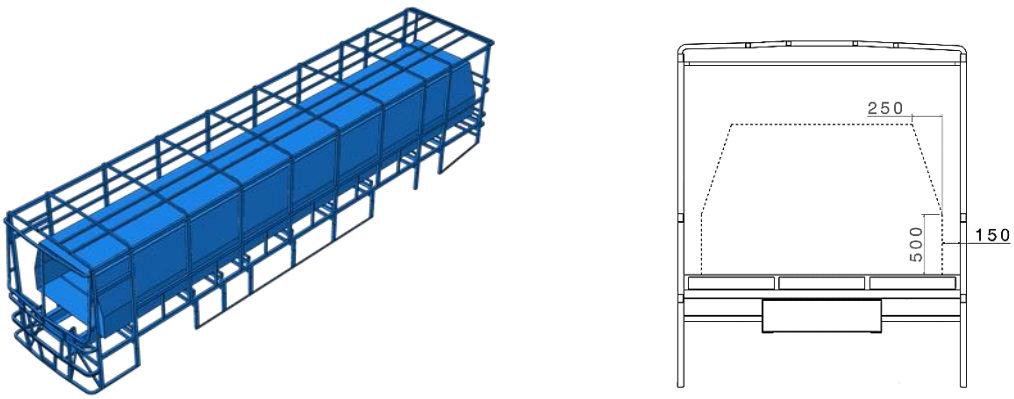

Figure 4-5, Residual Space (*all measurements are in (mm)*

The total size and weight of impacting trolley were taken from ECE-R95. The front section of the trolley has a cross-sectional size of 1.5 m by 0.5 m. This section is the main part that will be in contact with the side structure of the bus. Regulation has stated that the impactor side of the trolley is to be made by using a honey comp structure, which should be processed to give a progressively increasing level of force with an increase in deflection. In the current study, this section is taken as a solid block. But all other parameters like mass, speed, ground clearance and total size is as per the regulation. Figure 4-6 shows the general arrangement of the full bus structure and impacting trolley. The trolley was positioned at the center of the side structure, where it's close to the middle passengers' seat and fuel tank in opposite direction position. Crash testing the structure on this position will help in identifying the structure's ability to protect occupants and prevent fuel leakage due to impact. impactor speed is taken to be 48km/hr.

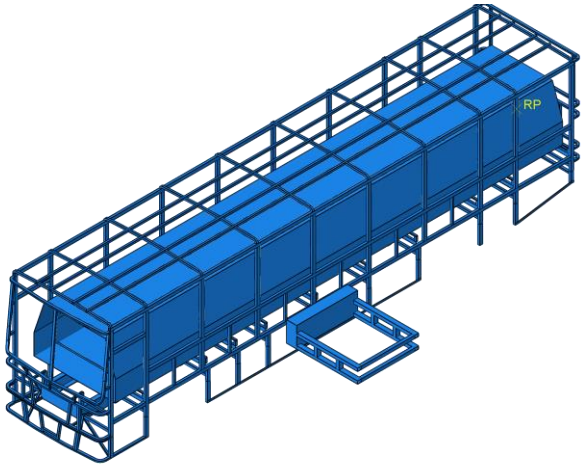

Figure 4-6, Side crash test arrangement

In addition to frontal and side crash tests, frontal-offset and side angle crash scenarios were analyzed for determining the crashworthiness of the structure. Offset frontal impact was giving the structure an initial velocity of 56 km/hr and crashing it with a rigid wall. The impact position will be on the left-hand side, where the driver is located. Analyzing the crashworthiness of the structure in this location will help in identifying the structure's ability to best protect occupants. For side angle impact impacting trolley is arranged in 27^{o} from the initial position on perpendicular impact. Figure 4-7 shows the arrangement of frontal-offset and side angled crash simulation setup.

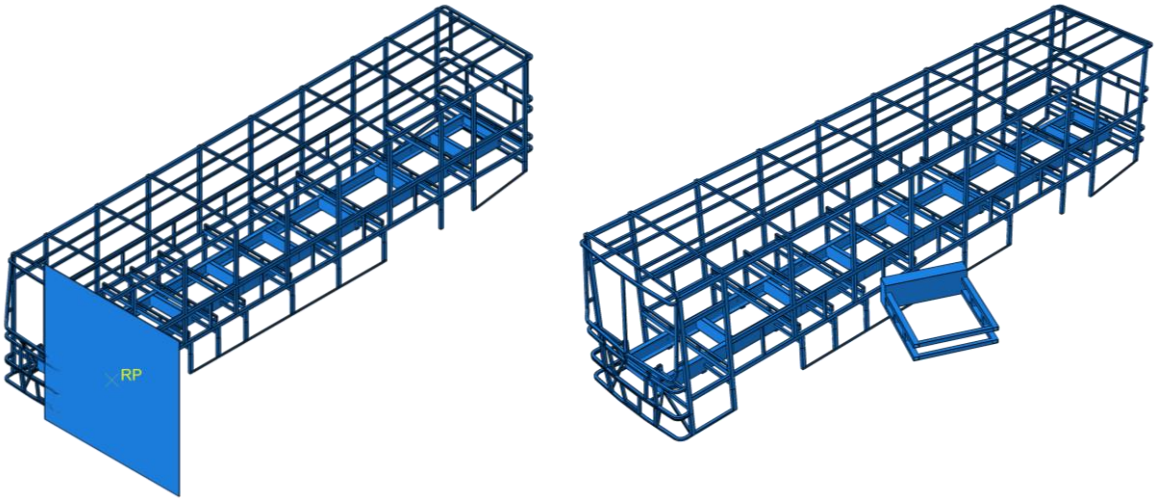

(a) (b)

Figure 4-7, Simulation set up (a) frontal offset crash and (b) side angled impact

4.2.1. Meshing

For the current study linear tetrahedron element was used for meshing. To have an adequate simulation result it's important to sufficiently refine the mesh. Using coarse mesh size will yield an incorrect result. By increasing the mesh density, the solution will converge to a specific value. After that further refining of the mesh will give minor changes in the solution. By using mesh convergence it's possible to conclude that the model used for the simulation will give a valid result. Mesh convergence can be done by using different parameters like energy, pressure, stress, reaction force, strain, and others in the system.

For the current study energy, abortion, and deformation in the structure are the prime consciences. But since the energy induced in the structure varies with an increase in time step, maximum strain energy induced in the system is alternatively to find the optimum mesh size.

Various global sizes are defined and strain energy is measured for each mesh size. Initial mesh size is selected by taking the maximum thickness of RHS steel used for the structure, which is 70mm, and decreased until the desired mesh size is found. Various global sizes with respective strain energy and several meshes are shown in table 4-3 and figure 4-8.

Global mesh size (mm)	No of Nodes	Strain energy (kJ)	Kinetic energy (kJ)
65	34443	13.027	55
60	37341	12.56	55
55	41034	12.23	55
50	45935	12.23	55
45	53361	11.85	55
40	63390	11.85	55
35	75493	11.85	55
25	146890	11.85	55

Table 4-3, Mesh convergence

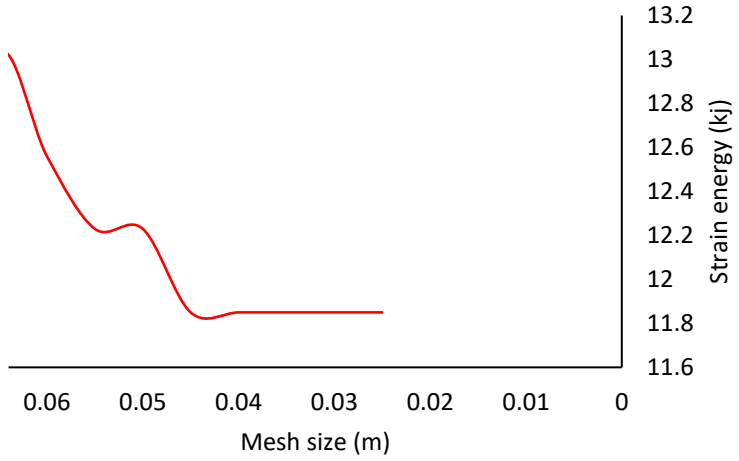

Figure 4-8, Stain energy vs mesh size

For different mesh sizes used on the model, the analysis result showed that the strain energy on the whole model starts to converge at an element size of 45 mm. For the current study, a global mesh size of 40 mm is adequate for simulation. further decreasing the mesh size will only increase simulation with a minor effect on desired results. By using this value, the front structure and complete superstructure were meshed by using 213,043 and 430,592 C3D4 elements.

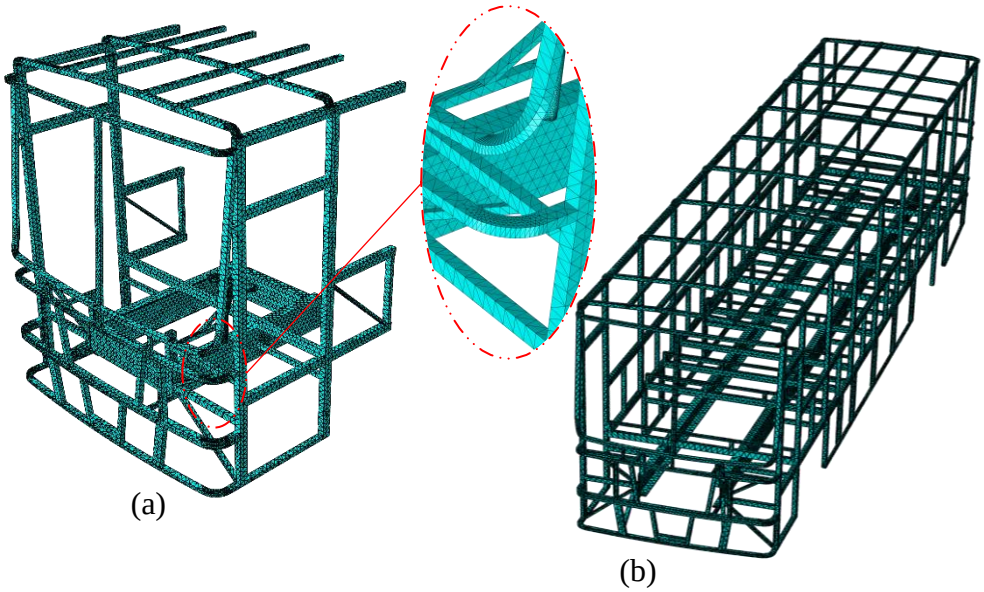

Figure 4-9, Meshing of (a) front structure and (b) full structure models

4.2.2. Analysis step

The steps for analysis are created by using the step module on ABAQUS. The procedure of the step was chosen to be Dynamic/Explicit with total simulation time of 0.035 starting from the structure contacting rigid plate or trolley in case of side impact until separation. Geometrical and other non-linearities were toggled on with the basic lab. By using equation 3-51 the critical/minimum time step increment for the simulation is found to be 9.8518e-10 sec. For a smooth simulation and ease of post-processing, the entire time of the crash event is divided into 50-time states with each step having all the output values at a specific time of the event.

4.2.3. Interaction

The contact definition was defined by using the contact property tool. Initially, mechanical tangential behavior with a penalty friction formulation was used for sliding friction. Normal behavior with hard contact is also defined. this will restrict friction to occur when the two parts are in contact only with separation after contact.

4.2.4. Boundary and Initial Conditions

The general boundary condition is based on ECE-R29 regulation for a frontal crash is used for simulation. The impactor is modeled as a rigid plate. End edges of the front structure model have a fixed end and the impactor will have an initial velocity. The regulations state that the impact should produce total kinetic energy of about 55 kJ. To produce this energy, The impactor

plate should have a tangential velocity of 8.071 m/s just before impact. For offset frontal impact the rigid wall has a fixed boundary condition while the complete structure is given an initial velocity of 56 km/hr (15.555 m/s) towards a rigid wall.

For side crash simulation fixed boundary was used on the chassis, where leaf spring hangers are located. This will create fixed support on four points leaving the rest of the structure. The test was done by giving impacting trolley an initial speed of 48 km/hr (13.333 m/s) [17] and collided with the structure in a perpendicular direction. In case of a side angle crash, the impacting trolley is positioned at angle whiles all other conditions are the same with perpendicular impact. impacting angle is taken to be 27^0 [25], which is taken from FMVSS 214 side-impact testing standard. The boundary condition for all crash scenarios is as shown in Figures 4-10.

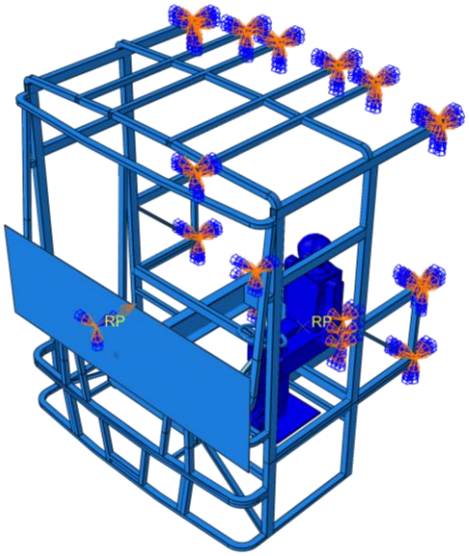

(a)

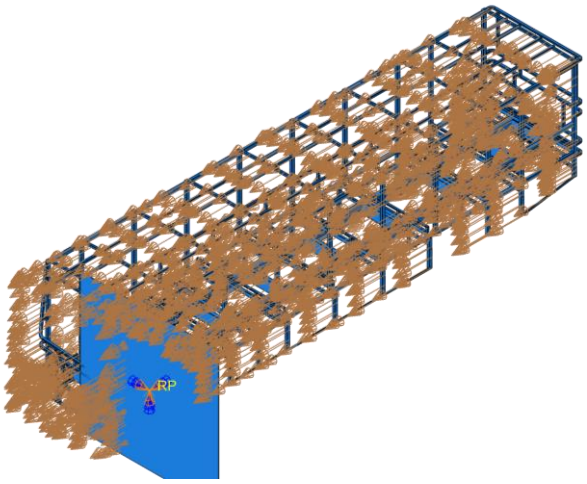

(b)

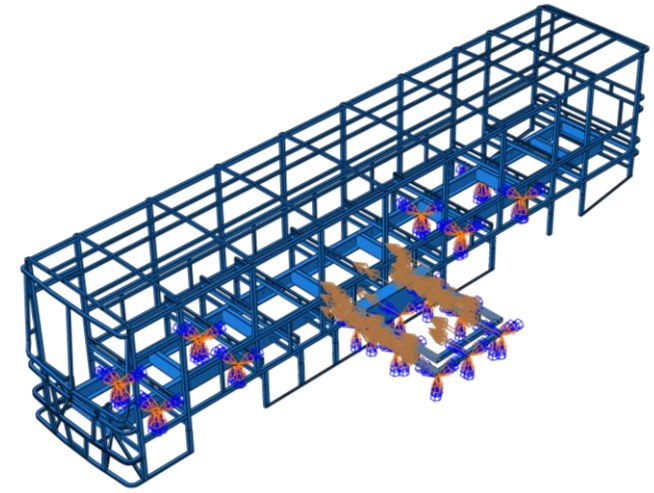

(c)

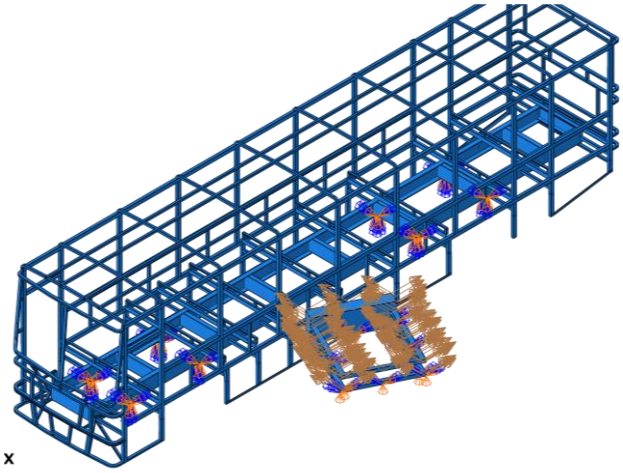

(d)

Figure 4-10, Boundary and initial condition setup (a) frontal crash test (b) frontal offset crash test and (c) side test and (d) side angled crash test

After setting all required preprocessing steps, the analysis was run and results for deformation, energy, crash pulse and other parameters are recorded. The results are presented by suing figures, chart and also by exporting to excel files. The results found are discussed in the next chapter.

CHAPTER FIVE:

5. Result and discussion

The result of the crashworthiness analysis of the bus structure in the case of frontal and side impact was illustrated in this chapter. The results include time history plots of deformation, velocity, energy, acceleration, crash force, and other parameters. Post-processing was done on ABAQUS for all types of impact conditions. The results obtained can be categories into two groups, as global /whole model value of energy, velocity, and acceleration and microscopic results like displacement, velocity, and acceleration of a selected node or element. The entire time of simulation was divided into 50-time steps in which all postprocessing outputs are given at a specific time of the event. The results are displayed by using shading and wireframe option, animation, contour plots, and vector plots. Four types of crash scenarios were performed on the structure of the bus.

- ✓ Frontal impact by using a rigid impactor
- ✓ Offset frontal impact with rigid wall
- ✓ Side perpendicular impact by impacting trolley
- ✓ Side angled/oblique impact by impacting trolley

5.1. Frontal impact

The front crash simulation of the bus per ECE-R29 standard is shown in figure 5-1. The rigid impactor is defined in front of the structure as illustrated in chapter 4. The impactor is positioned 15mm away from the front edge of bus frame. Impactor was given an initial velocity of 8,563.486 mm/s toward the front section.

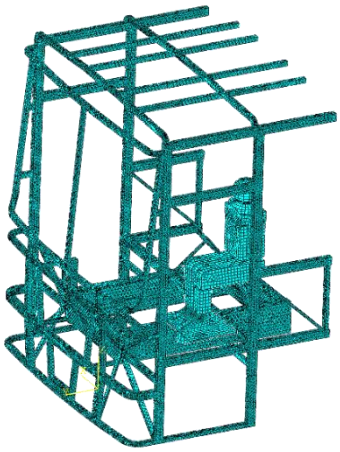

Figure 5-1, Front section of bus

Figure 5-2 shows the progressive deformation of the vehicle at different time steps. the impactor contacts frame at 0.00025s after the start of the simulation and separated after 0.03s. The simulation was terminated after 0.035 s. total time of the analysis was 759.9 CPU time. Deformation can be seen on the front frame of the bus. The total kinetic energy just before impact is 55 kJ. After the initial contact, the structure continued to deform until the separation of the impactor.

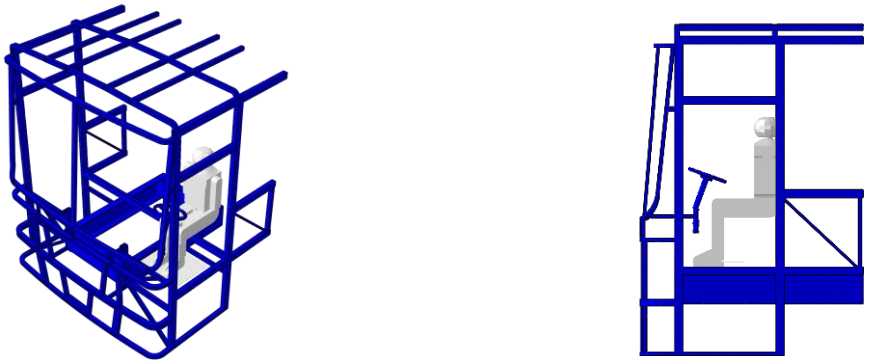

a) 0 sec

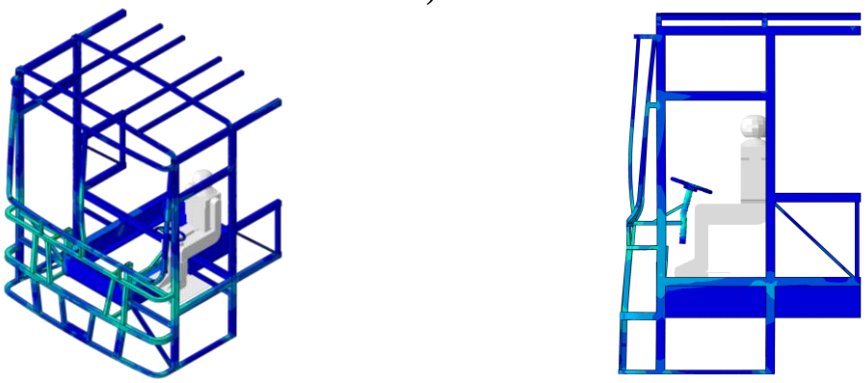

b) 0.01 sec

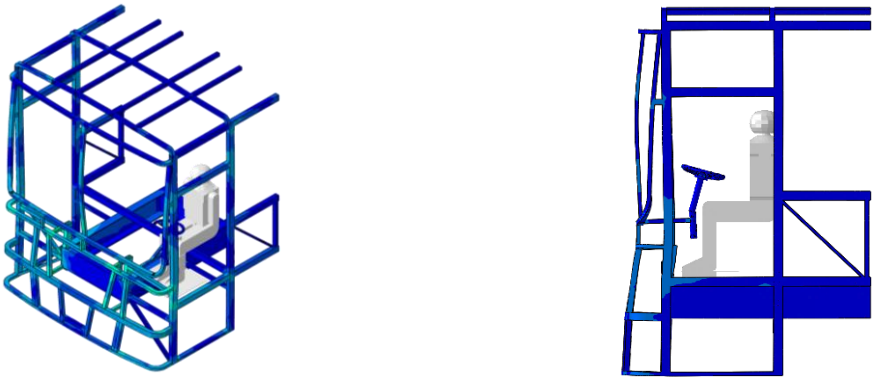

c) 0.02 sec

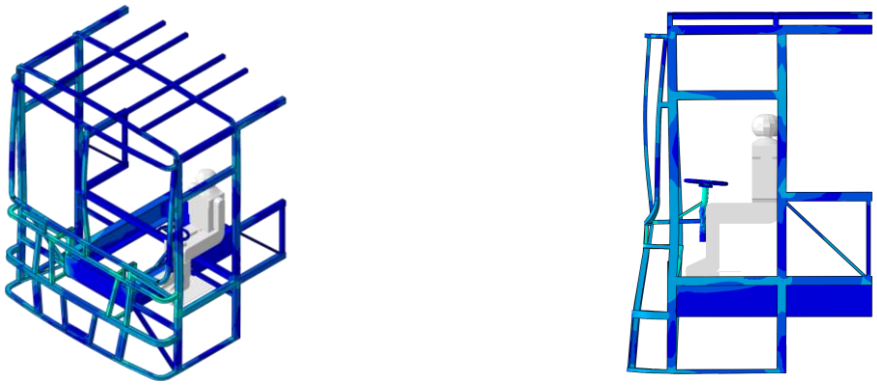

d) 0.03 sec

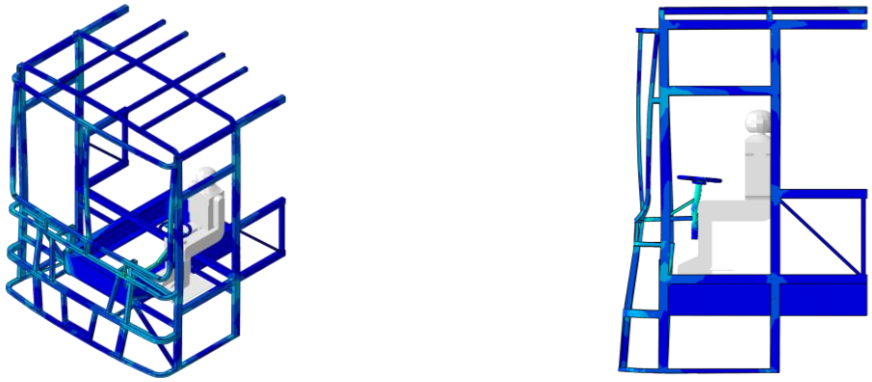

e) 0.035 sec

Figure 5-2, Progressive deformation in case of a frontal impact

As illustrated in Figures 5-2, bending of the front frame was observed just after the contact of impactor to front section any continues until separation of the two objects. The side pillars and front frame undergo a large bending deformation resulting from the impact. Also, the steering wheel is seen in contact with driver manikin with the lower section of the steering model intruding to the manikin. The maximum intrusion distance between the manikin and steering model during impact was found to be 17.235 mm. As seen in Figure 5-3, the steering model is seen in contact with the manikin which will result in injuries in the knee and chest area. The requirement for survival space specified in ECE-R29 regulation is not stratified.

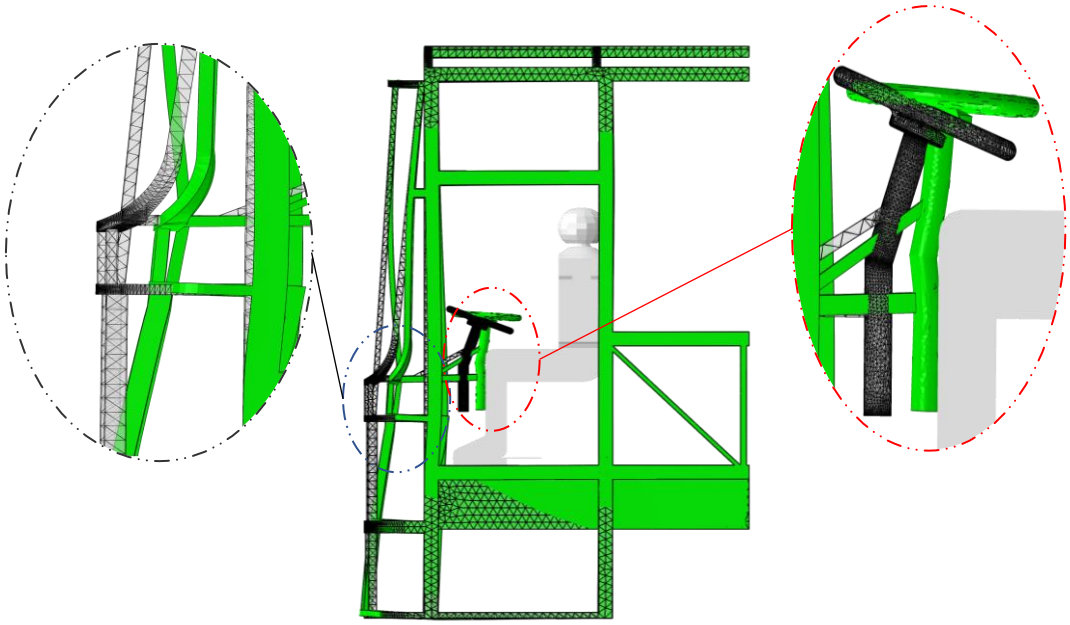

Figure 5-3, Undeformed and maximum deformation of front structure

Figure 5-4 shows the Von-Mises stress plot for the frontal section of the structure. The maximum stress induced in the structure is seen higher than the yield stress of the material. This shows that the deformation is in the plastic range and that material has yielded.

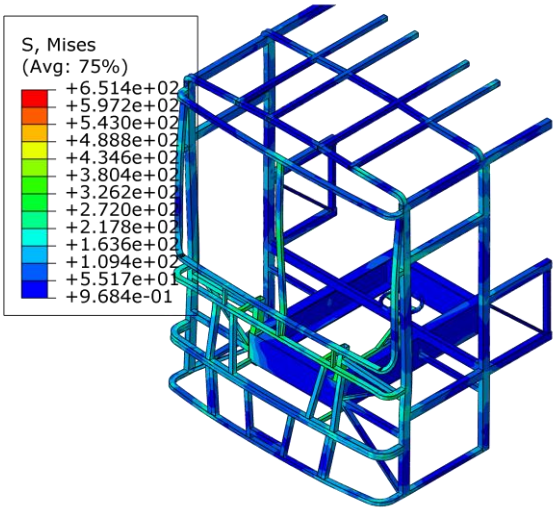

Figure 5-4, Von-Mises stress for frontal crash test (in MPa)

Maximum deformation of the front structure occurs at a time of 0.027 sec. Maximum deformation on the Front structure was found to be 122.34 mm. Figure 5-5, presents the frontal impact displacement of maximum deformed front frame, left & right-hand side pillars during the simulated process. Deflection on the front frame is seen as more severe than other structural components. Comparing the deflection of side pillars, the right-hand side pillar is seen as more

deformed than the left-hand pillar. The right-hand side pillar is where the passenger door is found and severe deflection is due to the lack of reinforcements as used on the left-hand side. This reinforcement is not used to have a space for passenger door on front right-hand side of the bus.

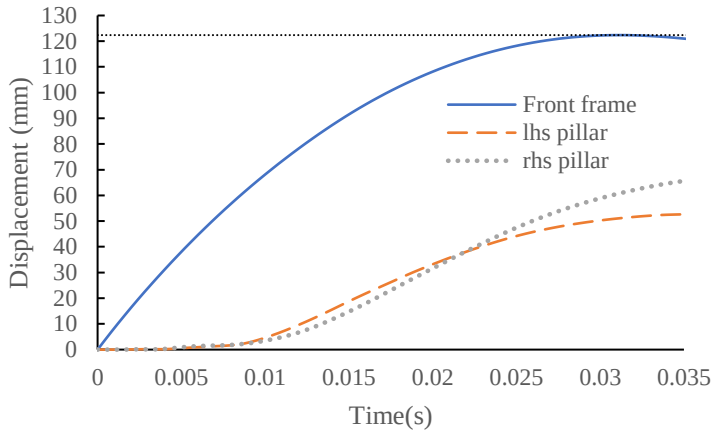

Figure 5-5, Deformation of main structures during impact

The pendulum crashes to the front frame of the bus first and crash energy progressively dissipates to the side pillars and back section of the model. Since the pendulum is in contact with the structure above the chassis less crash energy is seen transferring to the chassis. Energy balance in model versus time is shown in Figure 5-6. The total energy is seen to be constant during impact, which shows a suitable simulation and reliable result. The kinetic energy decreases gradually with time and tends to be stable after maximum deformation. The internal energy in the structure is seen to increase with time with a proportional rate as in kinetic energy.

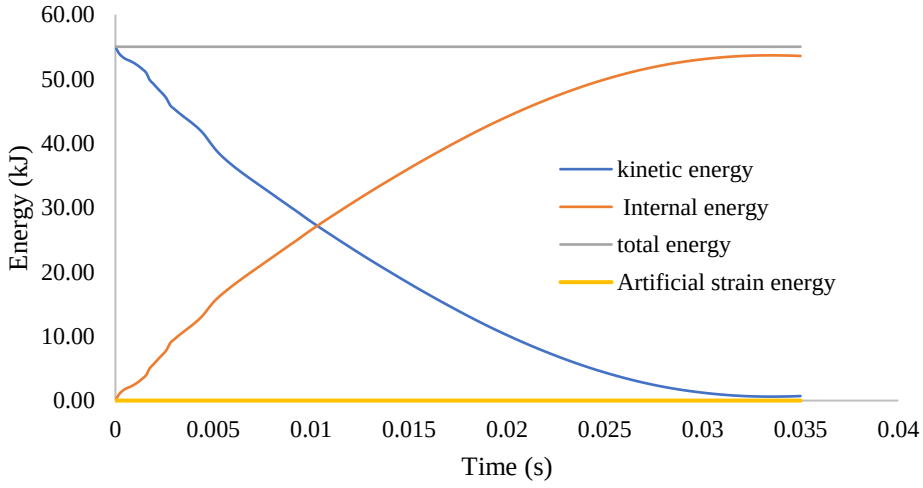

Figure 5-6, Energy balance for frontal impact

It can be seen that at time 0.035s the structure has absorbed all the kinetic energy during the impact process.

The artificial energy was used to validate that the response generated by the model meshing under loading conditions. The artificial strain energy in analysis was mainly used to supress and avoid the generation of the hourglass phenomenon. Usually the artificial strain energy must be less than 1% - 2% of the internal energy[17]. As shown in Figure 5-7 artificial strain energy amount is way below 1% of internal energy trough out the simulation.

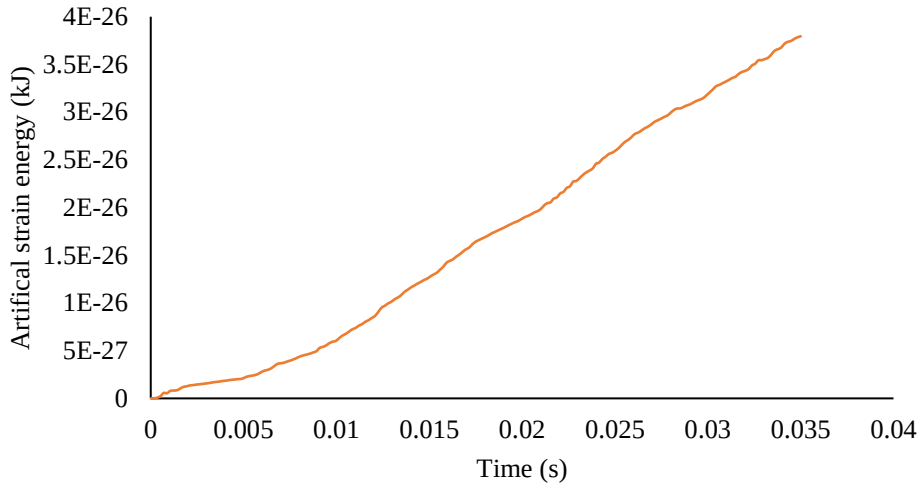

Figure 5-7, Artificial strain energy

Figure 5-7 presents the acceleration of the rigid impactor during the crash, also not that the peak value of the acceleration is around the first contact of the impactor. Impactor decelerates rapidly just after impact reaching a pick or lowest deceleration value after 0.0049 sec. During the crash time between 0.015 to 0.0325 s deceleration rate is seen almost constant and starts to decrease as the structure reaches maximum deformation. As the pick values are at the start of impact, it will cause occupants to rapidly move forward in the first instants of crash. Such kind of sudden movement will result in injuries to occupants. The mean acceleration during the impact can be computed by using the following equation [21].

$$a = \frac{v^2}{2g\Delta L} \qquad 5\text{-}1$$

Where, v is the translational velocity of the impactor, g gravitational acceleration, and ΔL total displacement of the structure.

For the current case, impactor velocity was 8.56 m/s and by using the total displacement of 122.34 mm. The mean and maximum crash pulse is found to be 26.029 g and 73.69 g

respectively. This value can also be found in the crash pulse plot given in Figures 5-8. A crash pulse is considered low when it's around 18g and is considered high for values around 87 g [21]. Considering total crash duration, the crush pulse value is at its lower range but the pick/maximum pulse is high for short period. By using eq. 3-6, the total HIC value was found to be 121.66 for 0.035 sec of crash time. The values to crash pulse are seen higher in the first instances of a crash up to 0.005 sec the value for HIC in this range is seen to be 119.01. These values are below the safe limit and head injuries to occupants will be minimum.

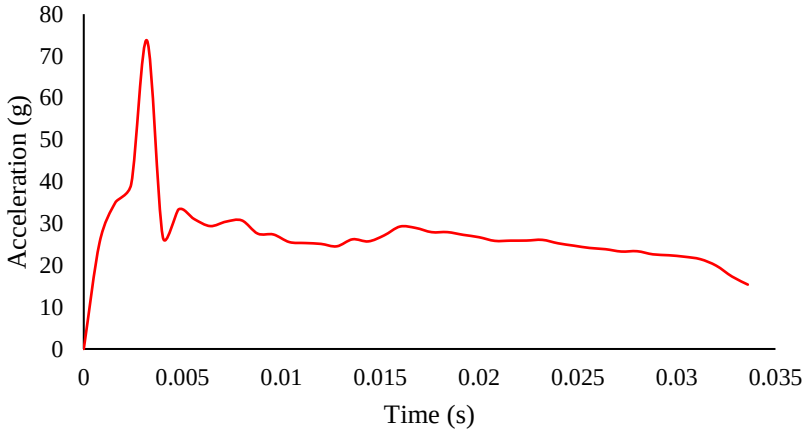

Figure 5-8, Acceleration of impactor in frontal impact test (g)

Crash force at the front section of the structure with respect to displacement is illustrated in Figures 5-9. By using equation 3-2 average crashing force is found to be 392.46 kN, this value also can be seen on the force and displacement graph. From the output data, the maximum crash force was about 1084.33 kN. From the force and displacement plot, we can find the total energy absorbed (E_{abs}) by the structure by using the equation as 53.87 kJ. This shows that out of 55 kJ of kinetic energy induced in the impactor about 97.9 % is absorbed by the structure.

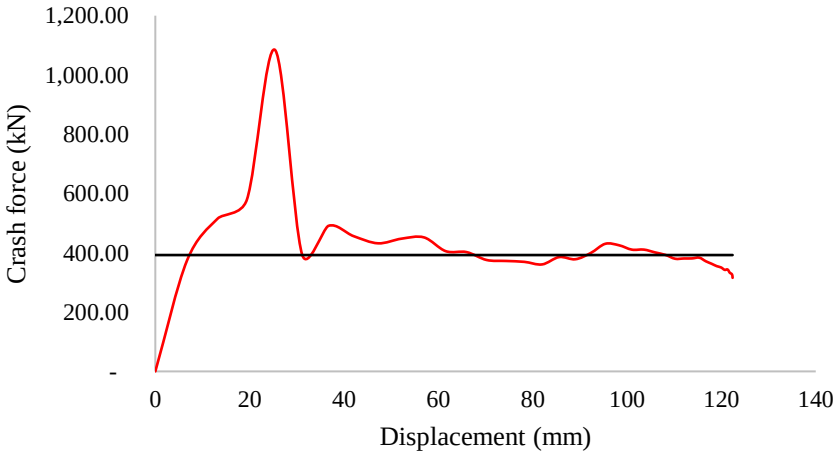

Figure 5-9, Crash force Vs displacement in the frontal impact test

By substituting the values for both average and maximum crash force into equation 3-5 crash force efficiency of the structure is found to be 0.36. For a proper cash performance, the value of CFE should be close to 1. For best crash absorbing ability value between 0.5 to 1 is more preferred. In the current case, the CFE value is much lower and indicating a sudden movement of occupants is just after impact.

5.2. Frontal offset impact

In addition to frontal impact, which is used to test crashworthiness of the structure under full frontal impact, the crash response of the structure under offset frontal crash was conducted. The general setup for the simulation is as discussed in chapter four. Total simulation time was 0.035 s starting from the first contact up to separation. With an initial velocity of the structure set at 56 km/hr (15.55 m/s) [8], the structure has generated 218.69 kJ of energy. Just after initial contact, the structure started to deform until the end of the simulation. Time step deformation of the structure is shown in Figure 5-9.

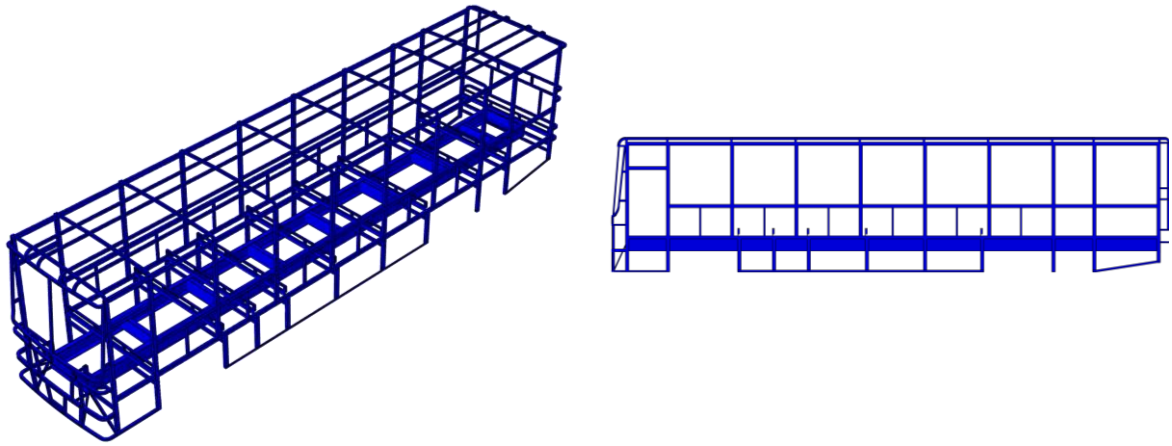

0 sec

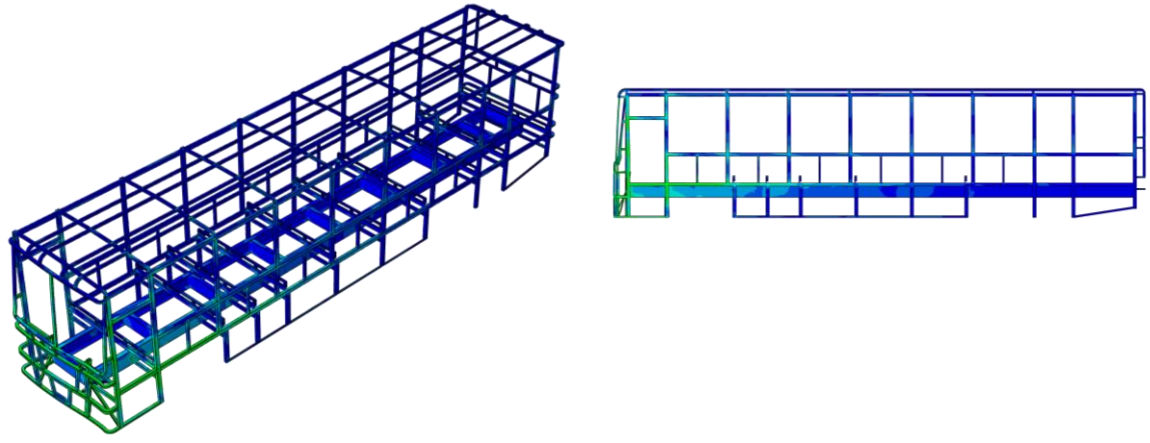

0.007 sec

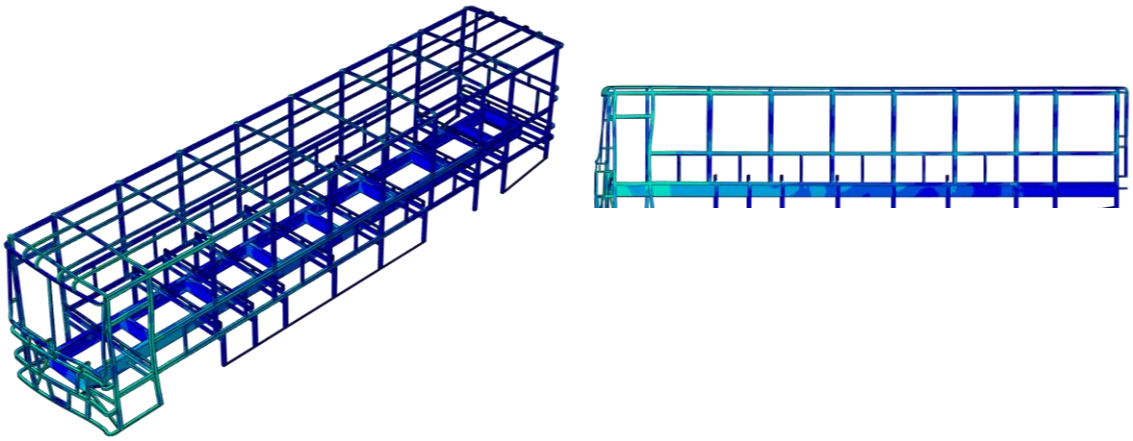

0.014 sec

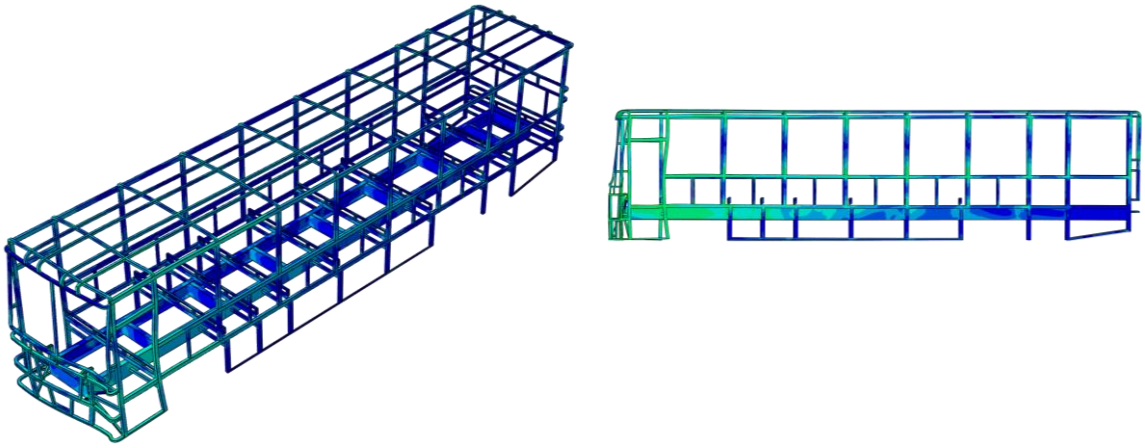

0.021 sec

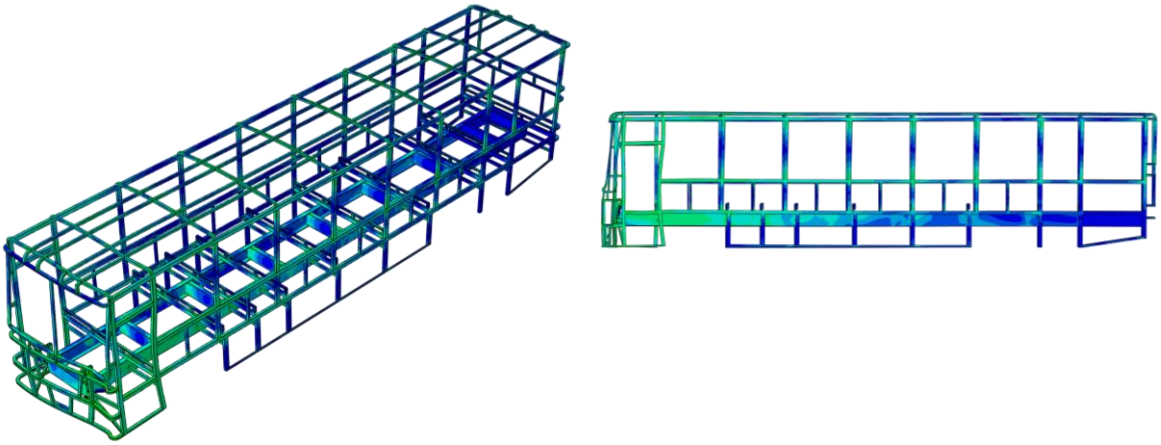

0.028 sec

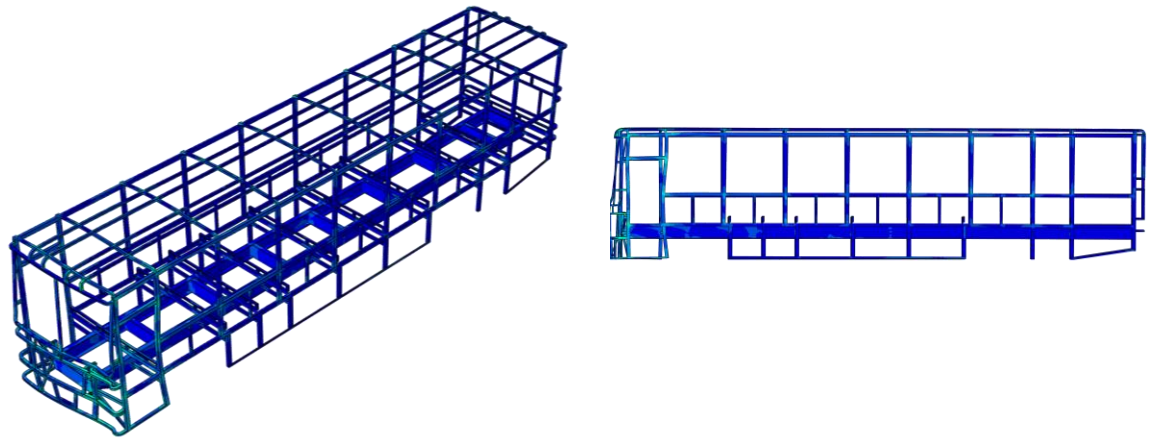

0.35 sec

Figure 5-10, Progressive deformation in offset frontal impact

The impact has caused high deformation on most components of the structure. The front structure mainly side pillars and roof undergoes severe bending, and the driver's safety will be severely compromised. The impact load is also seen to transmit to floor cross member and main chassis. The stress wave is seen to propagate starting from the front frame to the side members, roof, and rear section of the bus structure. high-stress concentrations are mainly observed on the front structure and side frames on connecting points. Frame connecting frames are made by

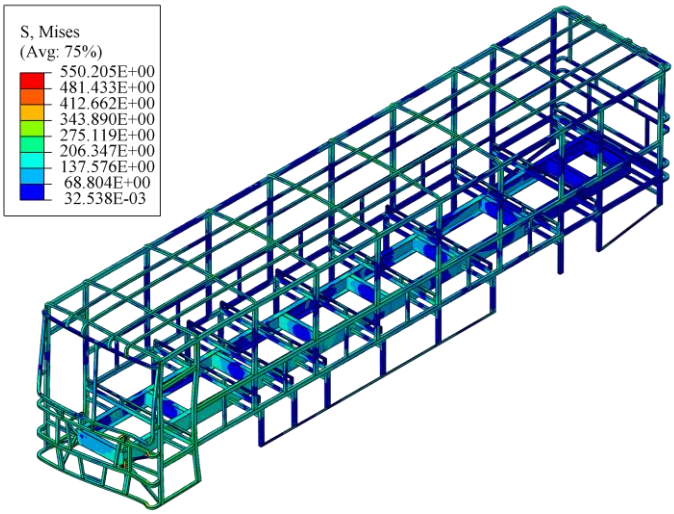

Figure 5-11, Von-Mises stress in frontal off set impact (in MPa)

using arc welding. Special emphasis Should be taken on welding to prevent the separation of welded parts and expose occupants to severe injuries. Such kind failures are observed on real accident photos as seen in figure 2-1. Maximum von-mises stress found was 550.2 MPa, which is more than the yield stress of the material, Figure 5-10 shows stress distribution and maximum stress.

Figure 5-11 shows the displacement of the front frames (windshield glass lower frame) during simulation. At maximum deformation was found at 0.0226 s with a total displacement of approximal 243.24 mm. deformation of front structure with such amount will cause injuries to the driver.

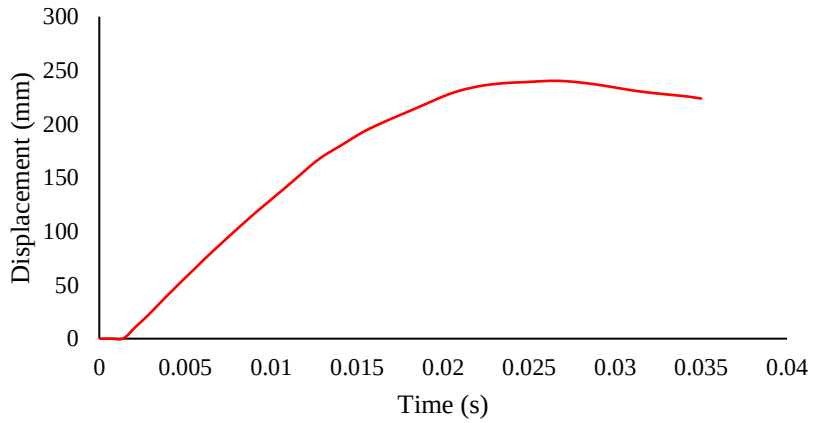

Figure 5-12, Displacement of front structure in offset frontal impact

The energy balance in the model is shown in Figure 5-11. The total energy is seen to be constant during impact, showing a suitable simulation and reliable result. As the kinetic energy decreases with time the internal energy in the structure is seen to increase and be maximum at a time where deformation of the structure is maximum. The maximum kinetic energy of the structure just before impact was found to be about 218.69 kJ. Artificial energy was used to validate that the response generated by the model meshing and its seen to be in minimum range.

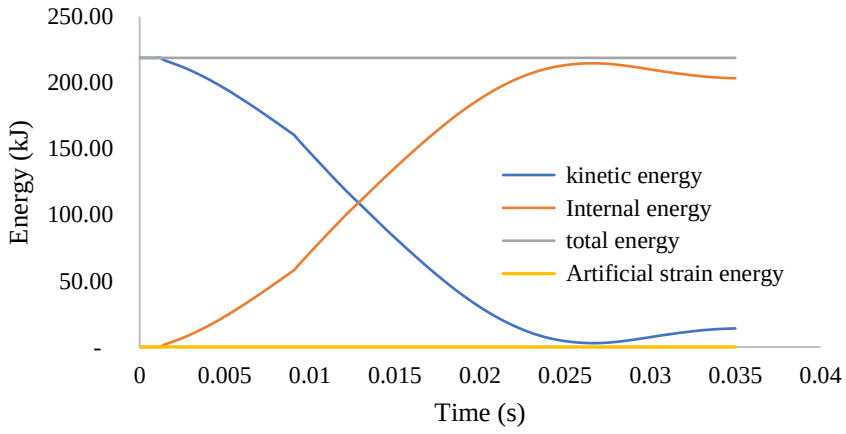

Figure 5-13, Energy balance in frontal-offset impact

Figure 5-14 presents the crash pulse of the structure during simulation, crash pulse values were taken from three different positions of the structure Front floor, middle floor, and rear floor. These positions are selected to occupants' seat acceleration as their seats are fixed with floor cross members. Selected points for crash pulse measurement are shown in Figure 5-13. Sever crash pulse is seen on all positions of measuring points. Such kind of excessive values will result in large displacement of occupants resulting in severe injuries. The highest peak crush pulses are seen on point 1, while pulses on points 2 and 3 are much lower. Crash pulse on driver location is seen much higher than the other points showing that the driver and occupants in the front section are susceptible to sustaining severe injuries.

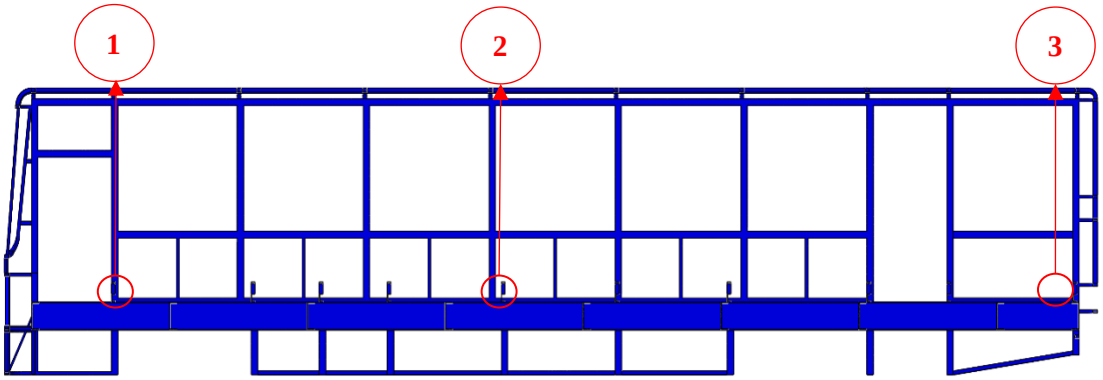

Figure 5-14, Crash pulse measuring points for frontal off set impact

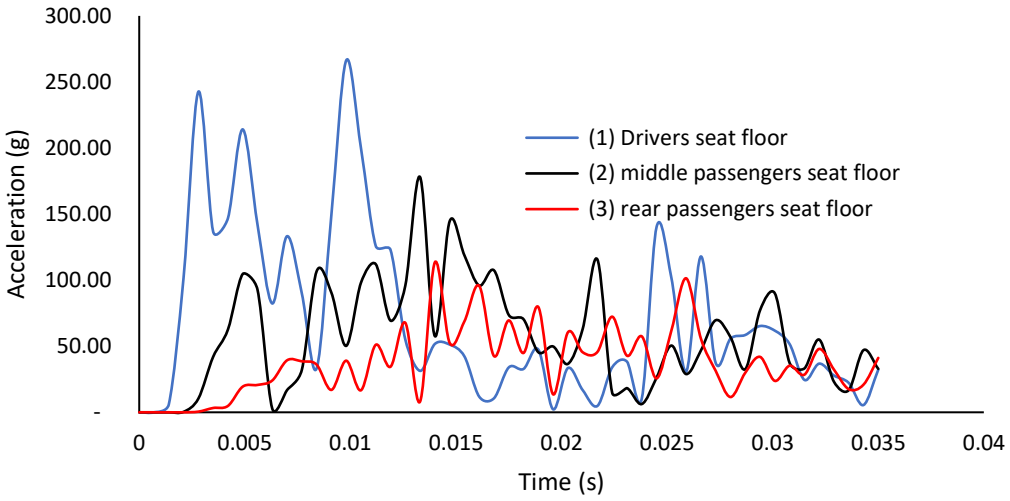

Figure 5-15, Deceleration of front structure part during offset frontal impact simulation

By using crash pulse data, the HIC value for each point was found to be 1,744.1, 859.2, 309.66 four points 1,2,3 respectively. As HIC value less than 1,000 are considered safe with minor or no neck injuries to occupants [11], occupants in middle and rear seats are less likely to encounter neck injuries compared with others. Although, the value of HIC for the middle section is seen lower than the safe limit it is seen much higher than the rear. HIC value at driver

point (driver seat floor) is way higher than the safe limit with potential for resulting in neck injuries on driver and occupants seating near to driver.

The reaction force on the rigid versus displacement of structure is shown in Figure 5-15. The maximum reaction force was 1,584.9 kN and average was found to be 967.14 kN. By using this values CFE is found to be 0.61. Such values show a good energy absorption with progressive deformation. About 98 % of total energy is seen absorbed by the bus structure with total absorbed energy of 214.59 kJ.

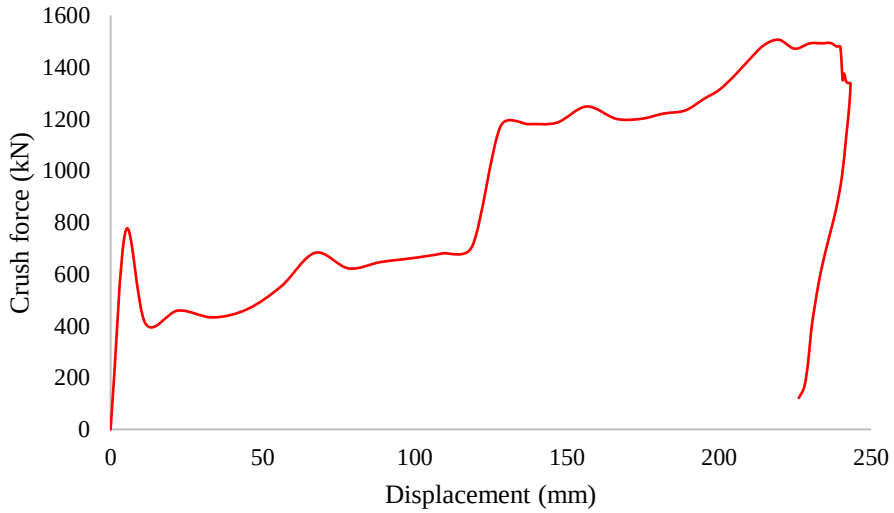

Figure 5-16, Crash force due to offset frontal impact

5.3. Side impact

In the case of the side impact test, the simulation was done for two different impact scenarios. Side perpendicular impact and angles impact. Impacting speed was set at 48 km/hr for both cases, with a total simulation time of 0.035, starting from initial contact to the final release of the impactor. The side structure started to deform after contact until the separation of impacting trolley. Figure 5-16 shows stress distribution in the structure; the results show that maximum stress is induced in the system in the case of perpendicular impact. This is because the contact area in a perpendicular crash is higher than side angled impact. also, the area of the structure affected by the crash is seen higher in the case of side perpendicular impact. The maximum stress in the structure is seen higher than yield stress in both crash conditions resulting in plastic deformation of the structure.

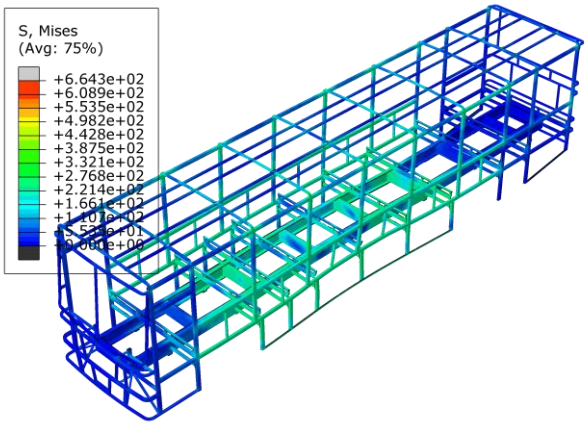

(a)

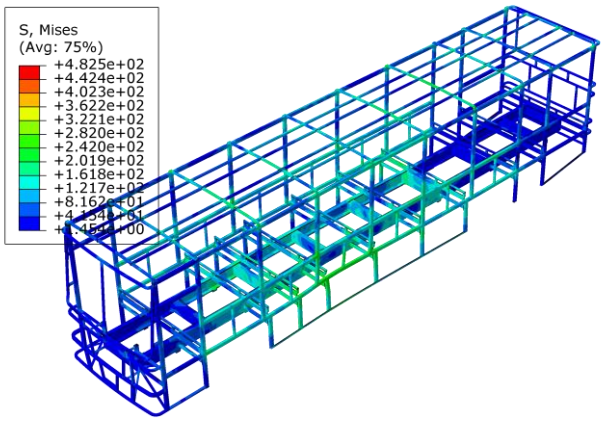

(b)

Figure 5-17, Maximum Von-Mises stress (MPa) (a) side perpendicular impact (b) side angle impact (in MPa)

The progressive deformation and stress distribution of the structure in both crash cases is as shown in Figure 5-17. Time step deformations are taken from the section of structure where the deformation is maximum for each crash simulation. By referring to the stress distribution, the impact load is seen to progressively transmit starting from the left-hand section to the right-hand section of the structure.

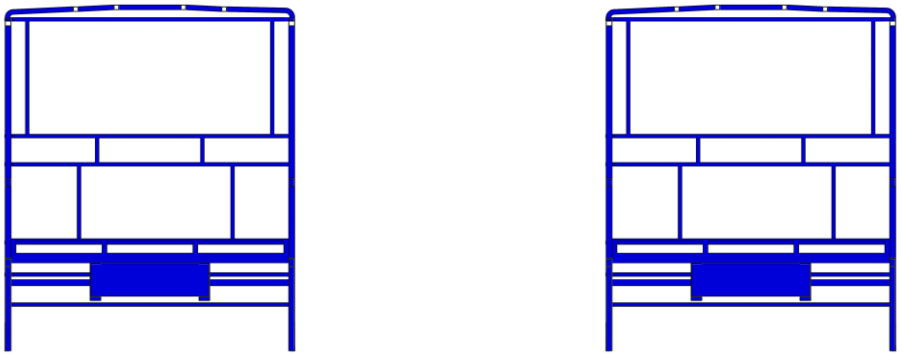

(a) 0sec **(b)**

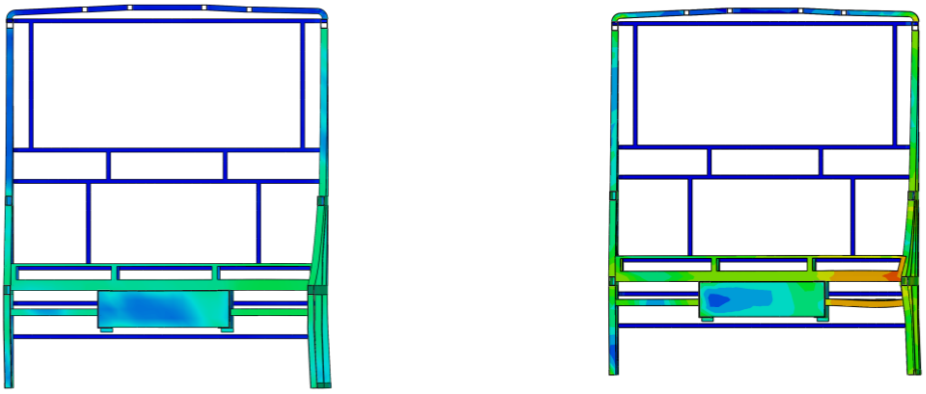

(a) 0.015 sec **(b)**

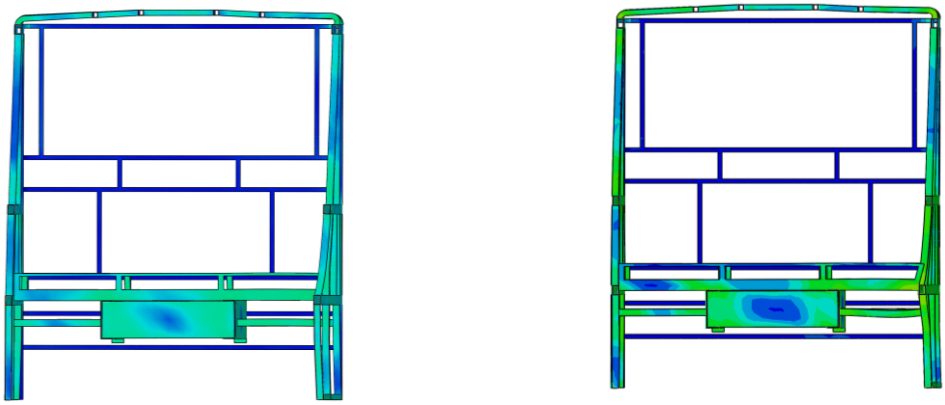

(a) 0.03 sec **(b)**

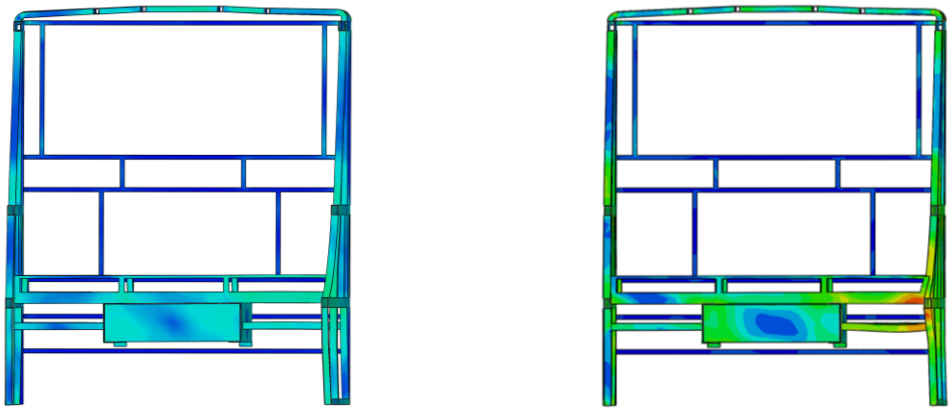

(a) 0.035 sec **(b)**

Figure 5-18, Progressive deformation on side crash simulation (a) side perpendicular impact, (b) side angled impact

Also, chassis and lower floor cross members are seen affected by the crash. Comparing the two results stress is more evenly distributed in case of a perpendicular crash while a stress concentration on a portion region is seen during side angled impact. the concentrated stress will create severe material damage on the contact point. In addition to stress distribution, minor buckling is seen on chassis and floor cross members in the case of side angled crash.

Maximum deformation of the side structure occurs approximately at time 0.03 sec during side perpendicular crash and 0.026 during side angle crash. Figure 5-18 shows the deformation rate of severely bent sections. Deformation of severely bent section starts right after impact and progressively increased in the case of perpendicular, while in angled impact, deformation of the highly bent pillar is seen to occur after a time of 0.0021 seconds after contact.

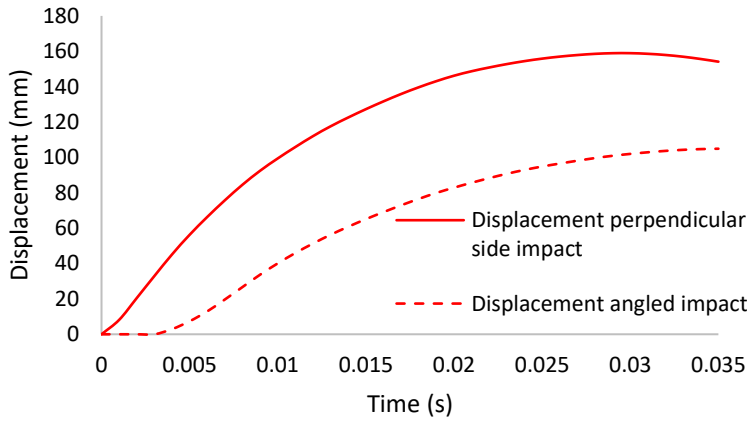

Figure 5-19, Displacement versus time graph of critical structure due to side impact

Taking node from the inner section of the structure where it's most deformed. It's seen that the maximum intrusion of the structure to the occupant's area is 158.92 mm and 105.07 mm in case of side perpendicular and side angled crash. To protect occupants from severe injuries, the clearance of residual space from the side structure was given as 150 mm during and after impact. Comparing those values, the side perpendicular crash has intruded the residual space by 8.92 mm. Such values of deformations will cause injuries to occupants. Figure 5-19 shows the deformation of structure relative to residual space.

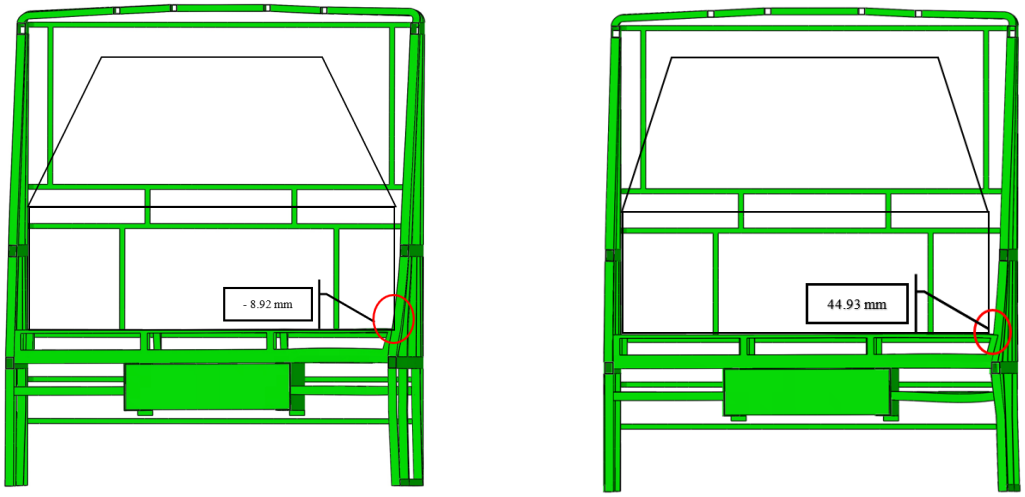

(a) (b)

Figure 5-20, Intrusion of side structure into residual space (a) Perpendicular side-impact (b) angled side impact

The energy graph in both crash models versus time is shown in Figure 5-20. It can be seen that the total energy remains constant during the crash, which shows that energy is conserved in the system. The results show that kinetic energy due to perpendicular side impact is seen high than side angled impact. In the side angled impact, the energy plot shows a sudden increase in internal energy of the structure just after impact and it gradually increases to its maximum and stable value.

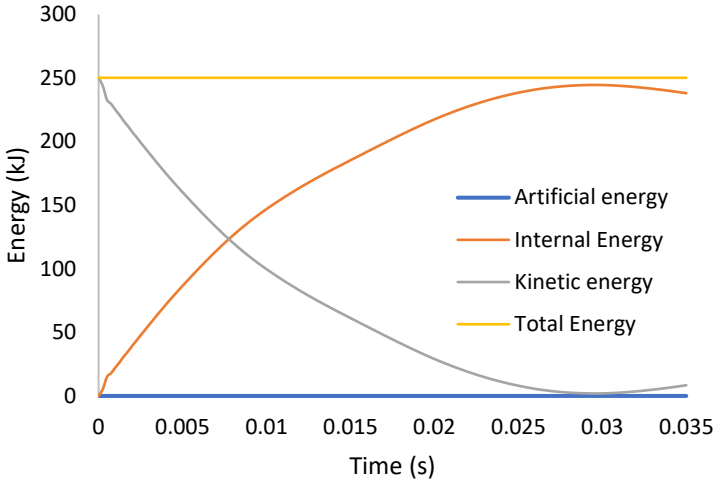

(a)

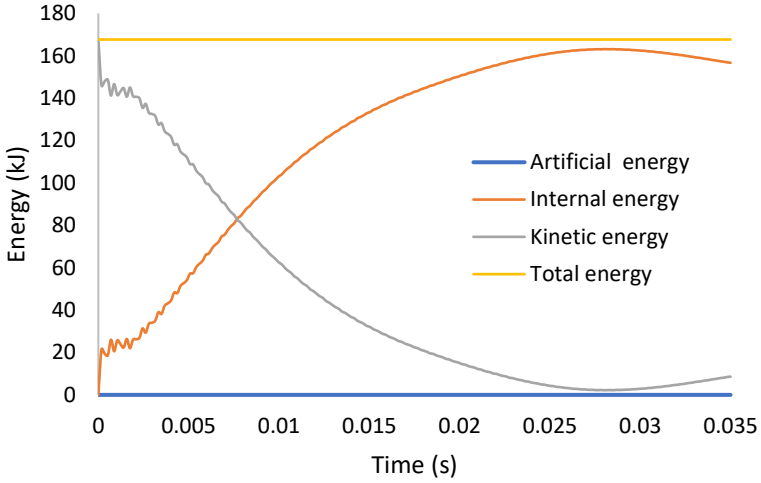

(b)

Figure 5-21, Energy Vs time graph, (a) side perpendicular crash (b) side angled impact

5.4. Improvement on crashworthiness of structure for Frontal Impact

The existing bus structure was numerically analyzed to determine the crashworthiness under frontal impact and side impact. Comparing the results for both impact cases base model sever structural deformation is seen in full frontal and offset frontal impact. One of the regulations used for studying the crashworthiness of the structure was ECE-R29 regulation for frontal-impact testing. The results showed that the current design doesn't pass ECE-R29 regulation, which requires the steering system to not intrude on the manikin and reserve safe space during impact. The structure failed in the front crash test resulting in damage in the driver's safe region with a maximum intrusion of 17.235 mm into the driver's manikin.

The results were used to identify the weaker structural components for improving crashworthiness. Accordingly, the front frames of the structure which holds the windshield

glass are seen to deform excessively. The structure's crash response can be adjusted by improving this section of the structure. The improvement implemented in the current study includes an increase in the thickness of the front frame and adding a reinforced profile. Such methods are seen to be effective in improving the response of the structure to crash [6] [22]. After adding those improvements, the crashworthiness is tested with the same procedure as in the frontal crash test shown in chapters four and five, which is based on ECE-R29 regulation.

To improve the crashworthiness for frontal impact three improvements are proposed and tested. In the first and second models, the improvement assumes that the deformation can be decreased by increasing the stiffness and rigidity of the front frame of the base model. As the front frame is seen to have higher deformation, increasing the thickness of those frames only is taken as the first alternative. This is achieved by increasing the thickness to 2.5mm from 2mm of front section frames. For the second model, the next structural sections seen to exhibit severe deformation were right-hand and left-hand side pillars (A-pillars). In addition to the thickness improvement seen on the first model, increasing the thickness of those sections to 3 mm from 2.5 mm might decrease the deformation.

For the third model, adding reinforcement for more axial load absorbing and decreasing deformation is considered. This is done by adding a reinforcement profile made out of 40×40×2 mm and 25×25×1.5 mm RHS just behind the front frame. The profile is added without affecting the space for mounting the dashboard and other accessories. Figure 6-1 shows the adjusted structure for all three cases.

The improvements are proposed by using easily available materials by local manufactures without changing the current external shape of bus. Other improvement methods like my changing material type, adding energy absorbing materials and changing the shape to accommodate crash box is not considered in the current study. The main goal of improvement is to show that safety of occupants can be improved by minor modifications.

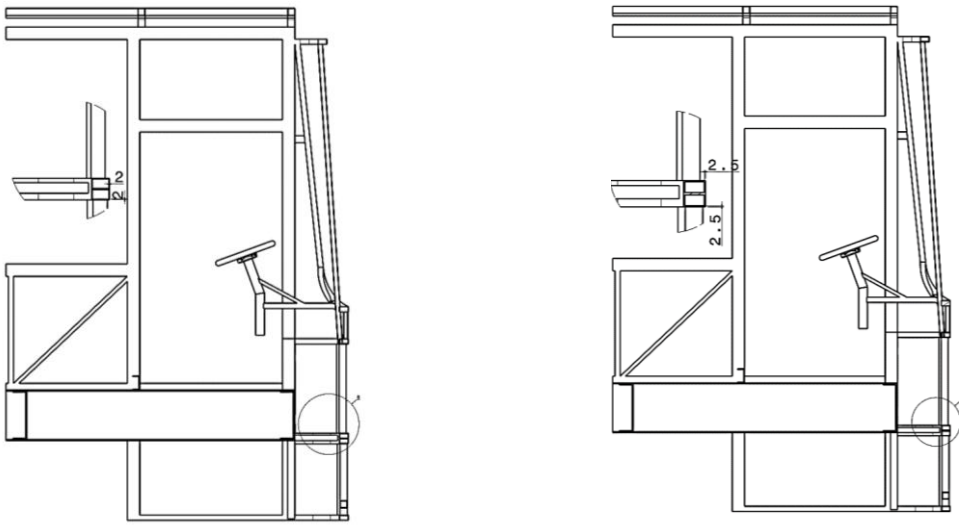

(a) Model 1, Structural improvement by changing the thickness of front frames only, baseline model in left side and improved model in right side

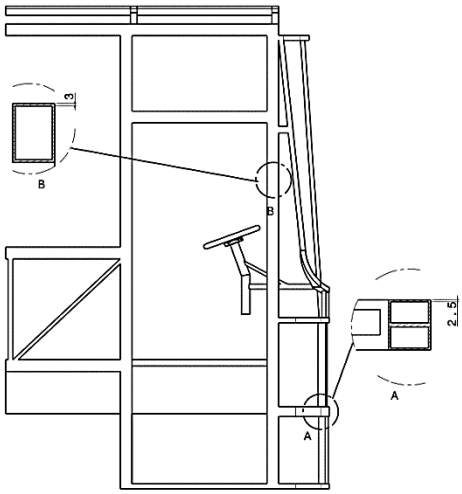

(b) Model 2, Structural improvement by changing the thickness of side pillars in addition to the front frame

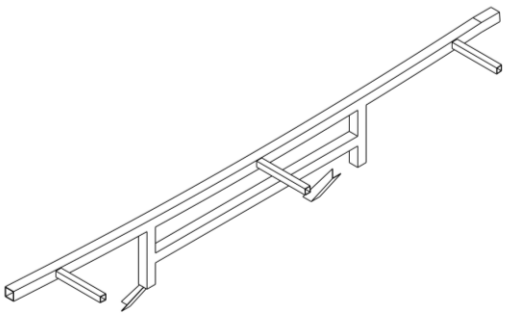

(c) Reinforcement profile

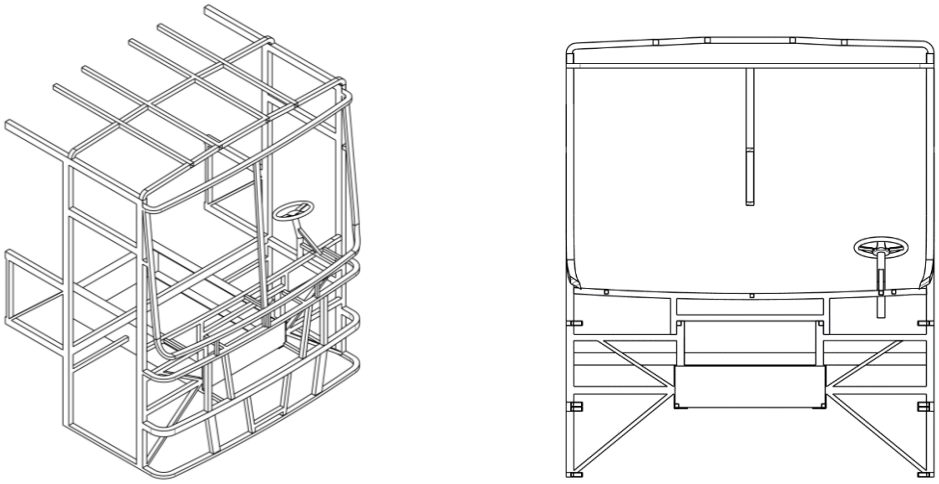

(d) Model 3, Isometric drawing of improved structure and section view of the front frame showing the added profile

Figure 5-22, Improved structure for all three models (*all dimensions are in mm*)

While implementing the above methods, the front structure mass is seen to increase in mass. The mass of the front structure is estimated to be 378 kg for model 1, 393 kg for model 2, and 388 kg for model 3. The baseline model had an estimated weight of 369 kg. The increase in mass of the structure is kept to be minimum.

Testing method and procedure were undertaken as discussed in chapter four. The results found are used to determine which method is more valid in satisfying the regulation and increasing driver's safety. After testing the results were used to check the distance between the manikin and steering model was measured for compliance with regulations. In addition to survivable space the crash force efficiency, energy absorbed, specific energy absorption capacity, and crush pulse are used for determining the crashworthiness of both models.

Total simulation time for all models were taken to be 0.035 sec. The total energy in all models was seen to be constant during simulation, showing a reliable result. The kinetic energy in both models is seen to decrease gradually while the internal energy increases. The total energy is seen to be constant and artificial energy is minimum validating that the results found by model mesh. Maximum energy absorbed by the system is found at time 0.0306 sec in model one,0.0265 sec for model two, and 0.0274 sec for model three.

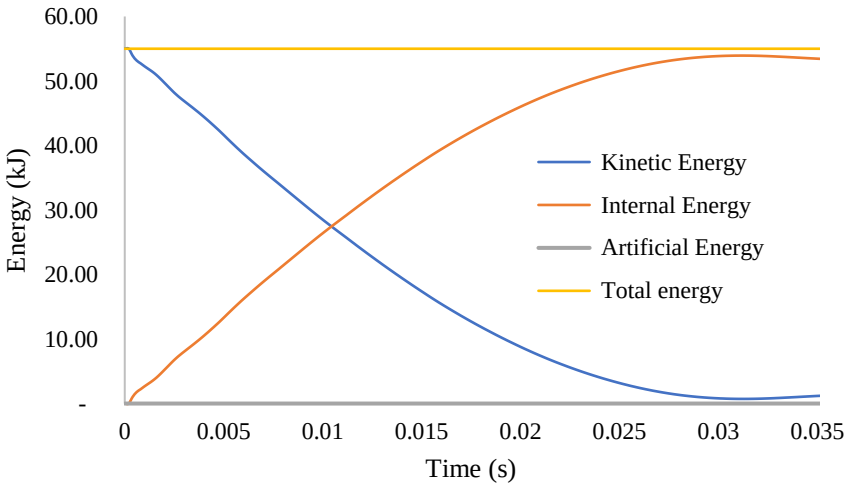

(a) Model 1

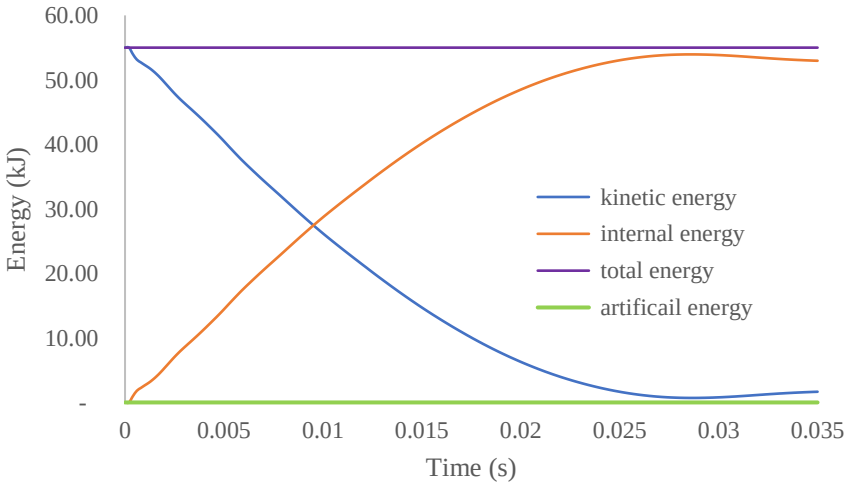

(b) Model 2

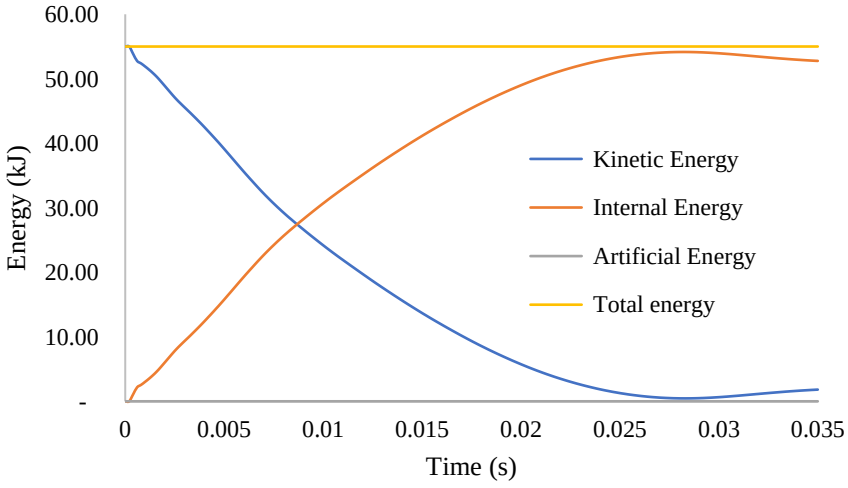

(c) Model 3

Figure 5-23, Energy balance for three models

Figure 6-3 shows the displacement of the front frame at each time instance during impact for all three models. The structure in the third model is seen to have less deformation compared to baseline and other models. The increase in stiffness and rigidity of the front frame only is seen to have less effect in decreasing the deformation of the structure. Additional thickness change of side pillars in model 2, has reduced deformation as compared with model 1. The improvement by reinforcing the front frame has yielded the smallest maximum deformation.

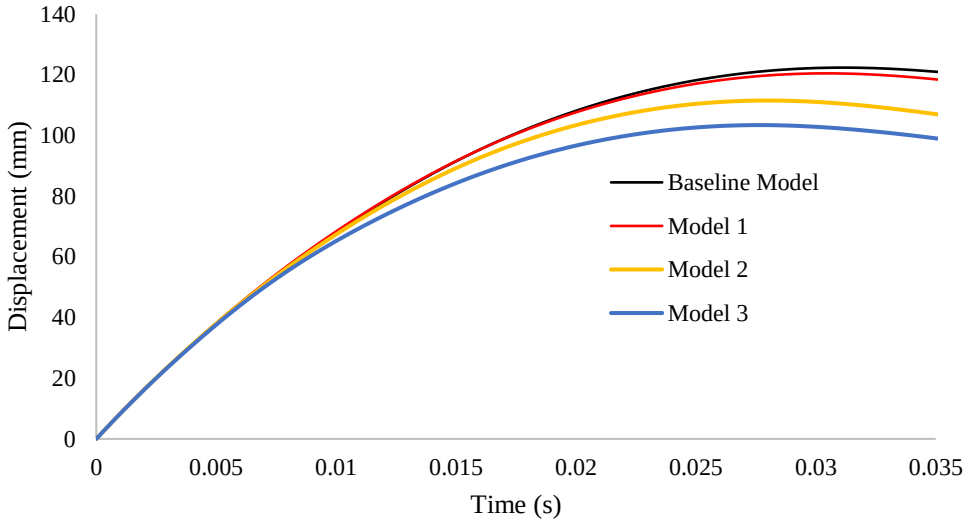

Figure 5-24, Displacement of the front frame for different models

The distance between the steering model and manikin is also compared for all three models. The results for the final position of the steering model relative to manikin are shown and summarized in Figure 6-4 and table 6-1. It was previously shown that in the baseline model the steering model has intruded the manikin by up to 17.235 mm. In model one by changing the material thickness of the front frame, the steering model has still intruded the manikin by up to 2.535 mm. In model two, the maximum displacement of the front frame is seen lower than the base model, Nevertheless, the steering model has an intrusion of 2.24 mm into manikin and failed to meet regulation. While in model three, the added reinforcement profile has significantly reduced the maximum displacement, and the steering model has not intruded or is seen in contact with the manikin. There is a 36.52 mm gap between the Steering model and the manikin, this is due to the additional protection of the front frame. Suh kind of gap will create a survivable space for driver and meet with regulation. Further adjusting the reinforcement profile will increase the gap between the steering model and manikin, and ensure driver safety.

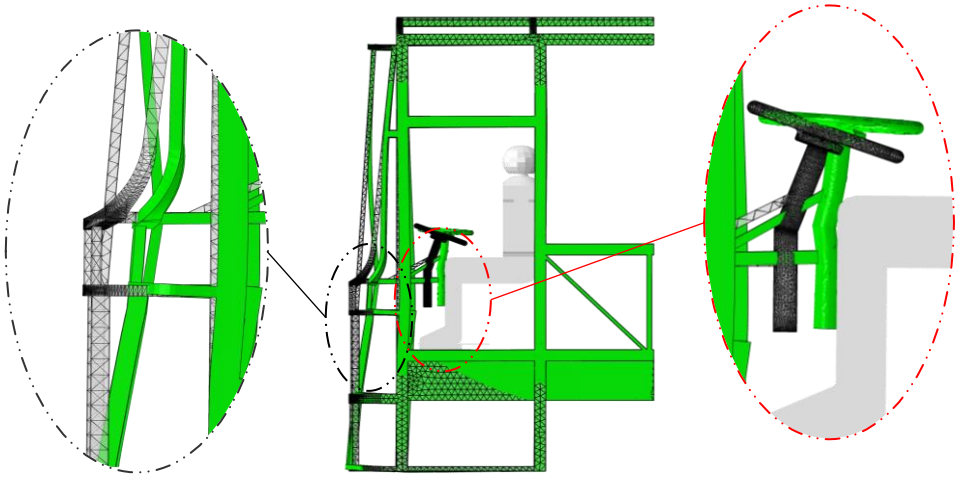

(a) Model 1

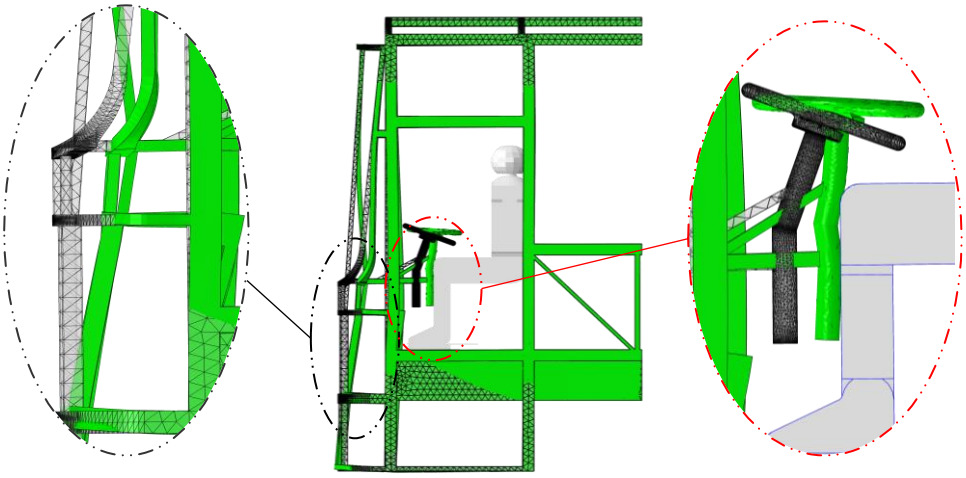

(b) Model 2

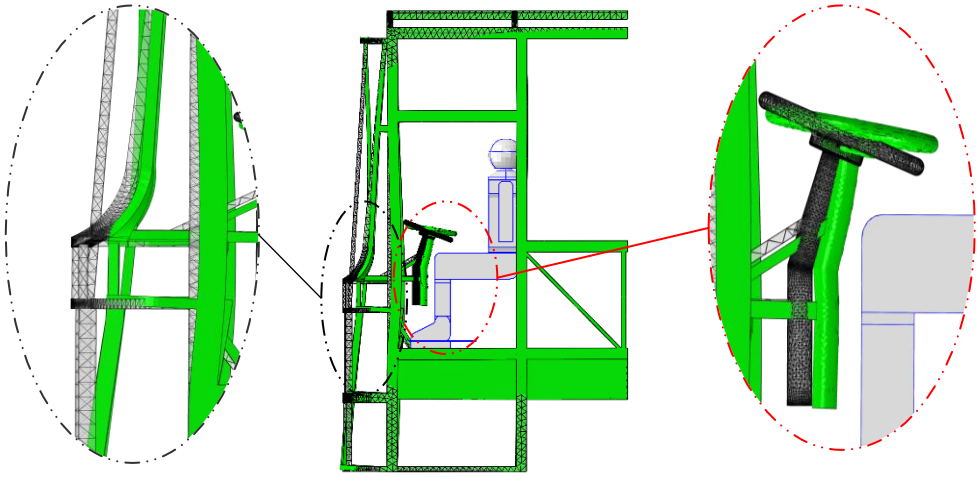

(c) Model 3

Figure 5-25, Deformed and undeformed shape of the improved models

Model	Maximum deformation (mm)	Clearance between manikin and steering system (mm)
baseline	122.369	-17.235
1	120.477	-2.535
2	111.52	-2.24
3	103.413	36.52

Table 5-1, Maximum deformation and clearance between manikin and steering model for different models (*minus sign shows intrusion of steering system to manikin)*

A comparison plot of crash pulse for all three models is shown in Figure 6-5. Baseline model has resulted in high acceleration peck, followed by an abrupt drop in acceleration. Peak crash pulse for baseline model is seen to occur just after impact, which will result in a sudden and severe movements of occupants. Pick crash pulse value observed on the baseline model is seen highly reduced by the modification to 40.58, 44.44, and 47.69 g for model one, model two, and model three respectively. The values show a reduction in sudden and severe movements of occupants during a frontal impact.

By using equation 3-6, HIC values for all three models were calculated and found to be 115.95, 128.53, and 125.49 respectively. HIC is seen close to the baseline model, which was found to be 121.67, and showing that the additional improvements will not cause the risk of occupants sustaining neck injuries. Although, the HIC value for the second and third models are seen a bit higher than the first model the values are still below the critical limit and head injury to occupants is less likely to occur.

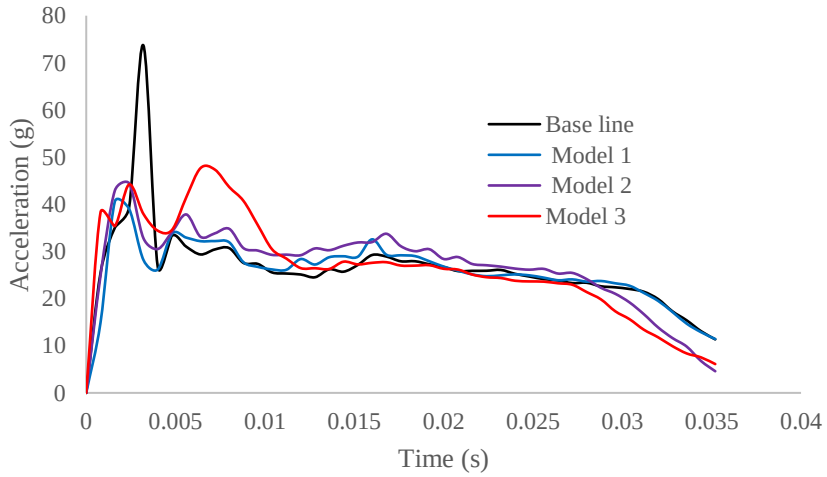

Figure 5-26, Acceleration/ Crush pulse of impactor for all for structure models

Crash force on the front structure for all three models is illustrated in Figure 6-6. Maximum crash force attained were found to be 597.16 kN, 435.95 kN, and 701.74 kN for model one, model two, and model three. While the average crash force for all models was found to be 277.16 kN,192.55 kN, and 286.06 kN respectively. By using these values, the crash force efficiency in improved models were found to be 0.49, 0.44, and 0.41 respectively. All three models had resulted in a higher crash force efficiency than the baseline model.

Referring to crash force plots the total energy absorbed by the structure in all cases were found to be 50.27 kJ, 51.79 kJ, and 51.51 kJ, which are 91.4%, 94.2%, and 93.13% of the total energy of 55 kJ, for model one, two and three respectively. As previously discussed the total energy absorbed by the baseline structure was 53.87 kJ (97.9 %). Comparing the results, increasing the thickness of the front frame only frame has lowered the energy-absorbing ability of the structure. while the additional thickness increases in model two and added reinforcement profile have resulted in absorbing relatively the same amount. Although, the total energy absorbed by the structure with added reinforcement profile is seen 4.8 % lower than the baseline model the structure has managed to absorb this value with much less deformation.

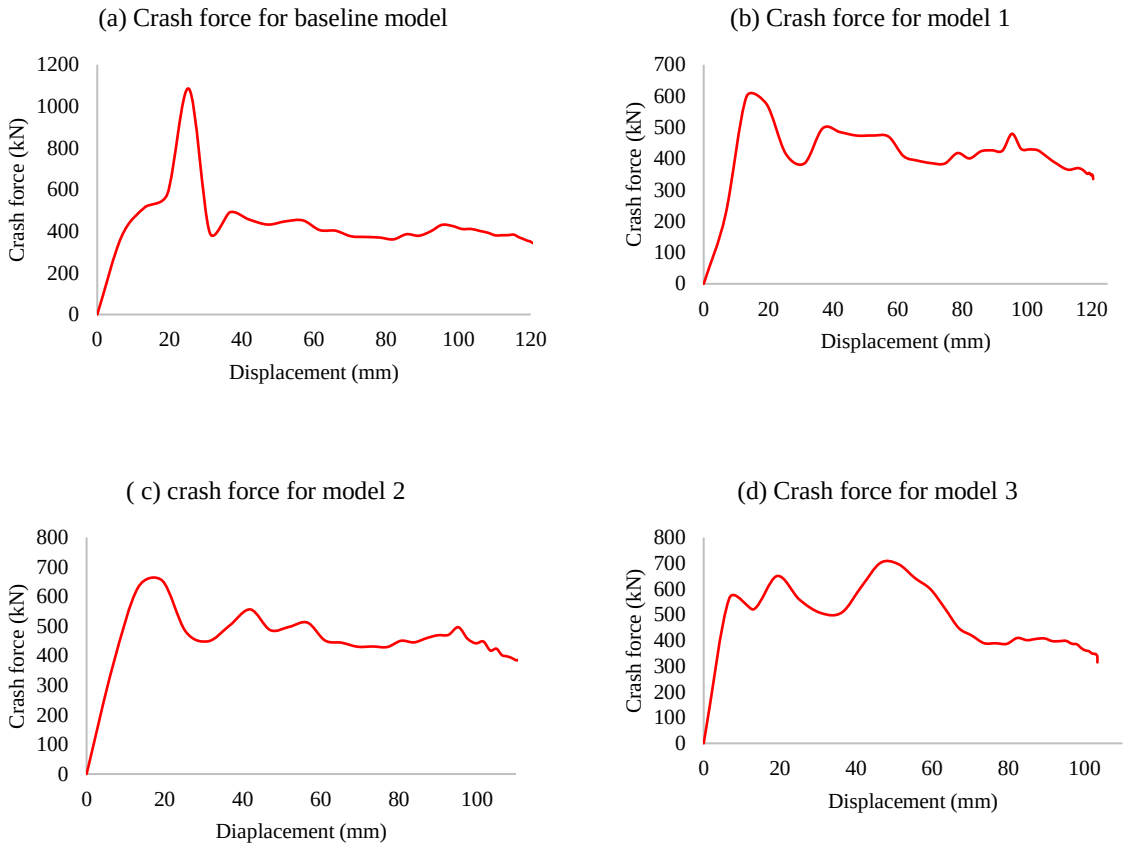

Figure 5-27, Crash force and displacement curve for all models

Crash force increase and decrease after the initial peak show progressive deformation of the structure. The third model has the highest number of peaks showing a progressive and controlled deformation.

Specific energy absorbed by three models was found to be 132.98 J/kg, 130.46 J/kg, and 132.75 J/kg for the model one, models two and three respectively. Although the Specific energy for all models is closely equal, improved models one and three are seen to be higher.

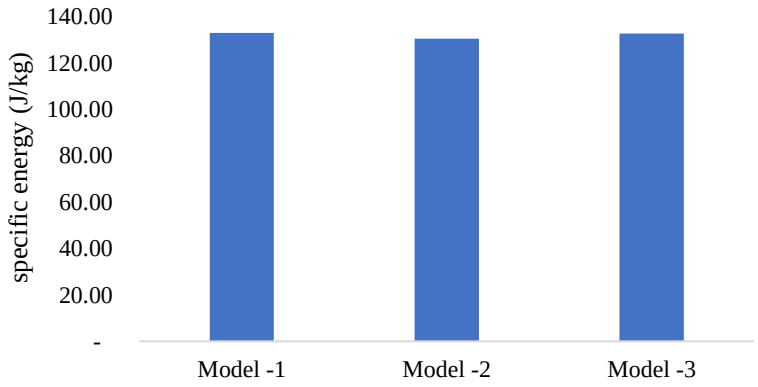

Figure 5-28, Specific energy for all models

Designing a crash worthy structure means providing protection for occupants in case of survivable collision [5]. Such kind of structures should have a peak load capacity to support energy absorbing members, with a minimum deformation. The compartment structure should also be an efficient energy absorbing structure that limits the compartment deceleration and the intrusion during crash. With this requirement, model three is seen to be more crashworthy with a good energy absorption capacity, lower deformation and high force.

In previous chapters, the crashworthiness of locally manufactured bus structured under ECE-R29 regulation was discussed. Accordingly, the results had shown that the current design failed to meet the regulation with an intrusion of the steering model into manikin of 17.23 mm. three improvement models were proposed for decreasing the intrusion distance and having a better structure that satisfies the regulation. The results have shown that the added reinforcing structure has increased the distance between manikin and the steering model. By adding a reinforcement profile, the crashworthiness of the structure can be improved and also meets requirement of ECE-R29 regulation.

CHAPTER SEVEN:

6. Conclusion and recommendation

6.1. Conclusion

After testing each impacting condition, the results were used to determine the most severe impact type from frontal and side-impact. Afterward, improvements on the structure were implemented for the severer affected sections of the structure for improved crashworthiness and the best alternative is recommended.

By analyzing the results found the following conclusions can be made from this study:

- The structure failed to meet ECE-R29 regulation with an intrusion of 17.235 mm of steering model to the manikin. The maximum deformation of the front structure was found to be 122.34 mm with an average crash force of 392.46 kN. The structure is seen to have a high energy absorption capacity by absorbing 97.9 % of 55 kJ kinetic energy induced by the impactor. Peak crash pulse had a value of 73.69 g, which is below the maximum value of the safe limit for occupant's injury range. HIC value of 119.01 was measured on structure as the result of the total crash pulse for 0.035 sec. This value is seen below the allowable range showing minor or no head injuries to driver/occupant in the front section of the bus structure.

- For offset frontal impact, severe deformation of the front frame and side pillars were observed with the highest displacement of 240.24 mm on the front frame. With initial velocity given to the structure total kinetic energy of 218.69 kJ was generated. Crash pulse induced in the structure was measured on three different points one on the drivers' floor, second on the middle floor, and third rear floor. Sever crash pulse was measured on driver area with a maximum crash pulse while the middle and rear have a lower value. Such kind of results shows that the impact will cause severe movement to driver and occupants on the front seat. HIC values for three measured crush pulses were calculated and found to be 1,744.1, 859.2, and 309.66. With the highest value seen on point taken from drivers' floor, which is much higher than the safe limit of 1,000 with a possibility of resulting in severe injuries to the neck of the driver and occupants near to driver. HIC values measured on the middle floor and rear floor are seen lower than the safe limit showing minor or no injuries to occupants in this area.

- Results for the side impact test showed that the structure has sustained a severe deformation in case of perpendicular impact up to 158.92 mm intruding residual space by 8.92 mm. although the intruded space is seen as minor, injuries to occupants are expected to occur.

- Comparing the crash test results for different impact positions. Frontal impacts are seen more severe with high structural deformation and lower occupants' safety. As a result, crashworthiness improvement is mainly focused on front structure. Three improved models for the front section of the bus structure were proposed. The first model focused on increasing the thickness of the highly deformed frame. The second model included additional thickness changes on side pillars of the bus, which were seen to exhibit deformation. For the third model, a reinforcement profile was added to increase the axial loading capacity of the front structure. The crashworthiness for all three models was tested following ECE-R29 and other parameters to select the best method.

- After comparing the results for the three models by adding a reinforcement profile has decreased the deformation of the structure much more than other models. Deformation was reduced to 103.41 mm, which is 15 % lower than the deformation seen on the initial structure. The improved structure has created a 36.52 mm gap between the steering model and manikin satisfying ECE-R29 regulation. Crash pulse due to the impact as significantly reduced with an average crash pulse of 47.69 g, which is much lower than the initial structure. Also, HIC was found to be lower than the safe limit.

6.2. Recommendation

A crashworthy bus structure plays a great role in protecting occupants during accidents and reduce injuries. In this study alternative approaches for increasing crashworthiness of 60 seated bus structure under frontal impact where proposed and tested. Final result had shown that by addition of reinforcement profile to preexisting design will reduce the deformation and reduce injuries to driver. The study recommends to adopt the findings of the research for a crashworthy bus structure.

6.3. Future research

As already stated, in this study, welding strength and defects were not considered. The structure was modeled as a continuous frame. Referring to real accident cases, in addition to structural deformation failure is seen to occur on welding joints. The strength of welding joints in different should be further studied.

The crashworthiness is tested in two impact positions, namely in frontal and side impacts. The structure's response under rear impact and rollover conditions should be studied. Also studying the crashworthiness of the 60 seated bus with full passengers will help in identifying the structures response in real case impact.

In addition, for further validation of the simulation results, another future work related to this study can be conducting an experimental test under ECE-R29 regulations.

Improvements on crashworthiness of front body structure are mainly based on easily available method like material thickness and reinforcement profile. Additional improvements can be studied by changing material type and adding an energy absorber like crash box.

Reference

[1] T. Megiso., "Optimization of Bus Body Building Methods by Investigation Of The Existing Problems And Rectification In Addis Ababa, Ethiopia.," *Int. J. Adv. Res.*, vol. 5, no. 2, pp. 1923–1938, Feb. 2017, doi: 10.21474/IJAR01/3362.

[2] Priti Gautam ; Robert Lisinge; Segni Getu; Yonas Bekele; Teferi Abegaz; Tilahun Gelete, "Road Safety Performance Review, Ethiopia," Geneva, 2020. [Online]. Available: http://creativecommons.org/licenses/by/3.0/igo/.

[3] J. A. C. Ambrósio and International Centre for Mechanical Sciences., "Crashworthiness : energy management and occupant protection," p. 466.

[4] J. Christensen and C. Bastien, "Nonlinear Optimization of Vehicle Safety Structures : Modeling of Structures Subjected to Large Deformations.," p. 488, 2015.

[5] P. Du Bois *et al., Vehicle Crashworthiness and Occupants Protection*. Southfiels, Michigan: Automotive Applications Committee American Iron and Steel Institute Southfield, Michigan, 2000.

[6] M. Huang, "Vehicle Crash Mechanics," Jun. 2002, doi: 10.1201/9781420041866.

[7] C. Gui, J. Bai, and W. Zuo, "Simplified crashworthiness method of automotive frame for conceptual design," *Thin-Walled Struct.*, vol. 131, pp. 324–335, Oct. 2018, doi: 10.1016/J.TWS.2018.07.005.

[8] P. Du Bois *et al.*, "Vehicle Crashworthiness and Occupant Protection."

[9] R. A. Galganski, "Crashworthiness design of HSGGT vehicles," *Tech. Pap. - IEEE/ASME Jt. Railr. Conf.*, pp. 121–130, 1993, doi: 10.1109/RRCON.1993.292954.

[10] T. L. Teng, P. H. Chang, C. C. Liang, and D. A. Fung, "Application of crash pulse on the car crashworthiness design:," *https://doi.org/10.1177/1687814017700096*, vol. 9, no. 9, pp. 1–8, Sep. 2017, doi: 10.1177/1687814017700096.

[11] J. A. NEWMAN, "Head Injury Criteria in Automotive Crash Testing," 1980.

[12] P. Wriggers, "Nonlinear finite element methods," *Nonlinear Finite Elem. Methods*, pp. 1–559, 2008, doi: 10.1007/978-3-540-71001-1.

[13] L. Kwasniewski, H. Li, R. Nimbalkar, and J. Wekezer, "Crashworthiness assessment of

a paratransit bus," *Int. J. Impact Eng.*, vol. 5, no. 32, pp. 883–888, May 2006, doi: 10.1016/J.IJIMPENG.2005.03.007.

[14] C. C. Liang and G. N. Le, "Bus rollover crashworthiness under European standard: an optimal analysis of superstructure strength using successive response surface method," *http://dx.doi.org/10.1080/13588260902920670*, vol. 14, no. 6, pp. 623–639, Dec. 2009, doi: 10.1080/13588260902920670.

[15] D. Abellán-López, M. Sánchez-Lozano, and L. Martínez-Sáez, "Frontal crashworthiness characterisation of a vehicle segment using curve comparison metrics," *Accid. Anal. Prev.*, vol. 117, pp. 136–144, Aug. 2018, doi: 10.1016/J.AAP.2018.04.017.

[16] A. D. de Meira, I. Iturrioz, M. Walber, and F. Goedel, "Numerical Analysis of an Intercity Bus Structure: A Simple Unifilar Model Proposal to Assess Frontal and Semifrontal Crash Scenarios," *Lat. Am. J. Solids Struct.*, vol. 13, no. 9, pp. 1616–1640, 2016, doi: 10.1590/1679-78252440.

[17] H. Wang, D. Xiang, L. Jiang, G. Duan, and H. Zhang, "Improvement of Vehicle Crashworthiness for Full Frontal Impact Based on Energy Flow Analysis," *Adv. Mater. Res.*, vol. 139–141, pp. 1365–1369, 2010, doi: 10.4028/WWW.SCIENTIFIC.NET/AMR.139-141.1365.

[18] M. A. Güler, M. E. Cerit, S. K. Mert, and E. Acar, "Experimental and numerical study on the crashworthiness evaluation of an intercity coach under frontal impact conditions," *Proc. Inst. Mech. Eng. Part D J. Automob. Eng.*, vol. 234, no. 13, pp. 3026–3041, Nov. 2020, doi: 10.1177/0954407020927644.

[19] M. A. A. Afripin, A. Z. Zainudin, M. A. H. F. M. Sahar, and M. Yusof, "Frontal impact on bus superstructure as per UNECE R29 and NCAP," *IOP Conf. Ser. Mater. Sci. Eng.*, vol. 670, no. 1, p. 012014, Nov. 2019, doi: 10.1088/1757-899X/670/1/012014.

[20] M. F. Horstemeyer *et al.*, "Material and structural crashworthiness characterization of paratransit buses," *http://dx.doi.org/10.1080/13588260701483680*, vol. 12, no. 5, pp. 509–520, 2007, doi: 10.1080/13588260701483680.

[21] P. Jongpradist, S. Senawat, and B. Muangto, "Improvement of Crashworthiness of Bus Structure under Frontal Impact *," 2015.

[22] W. Wen-wei, Z. Cheng-jun, and C. Jiao-yang, "Pure Electric Bus Crashworthiness

Analysis," pp. 89–92, Dec. 2012, doi: 10.2991/MEMS.2012.23.

[23] C. Bojanowski and R. F. Kulak, "Multi-objective optimisation and sensitivity analysis of a paratransit bus structure for rollover and side impact tests," *http://dx.doi.org/10.1080/13588265.2011.616118*, vol. 16, no. 6, pp. 665–676, Dec. 2011, doi: 10.1080/13588265.2011.616118.

[24] G. V. Mariotti, "Head Injury Criterion: Mini Review," *Am. J. Biomed. Sci. Res.*, vol. 5, no. 5, pp. 406–407, Oct. 2019, doi: 10.34297/AJBSR.2019.05.000957.

[25] C. M.Harris, *Shock and Viberation Handbook*, 5th ed. McGraw-Hill, 2002.

[26] M. Cerit, M. A. Guler, B. Bayram, and ur Yolum, "Improvement of the Energy Absorption Capacity of an Intercity Coach for Frontal Crash Accidents," 2010.

[27] "Mild Steel | Density, Strength, Hardness, Melting Point." https://material-properties.org/mild-steel-density-strength-hardness-melting-point/ (accessed Nov. 21, 2021).

[28] K. Vedantam, D. Bajaj, N. S. Brar, and S. Hill, "Johnson - Cook Strength Models for Mild and DP 590 Steels," *AIP Conf. Proc.*, vol. 845, no. 1, p. 775, Aug. 2006, doi: 10.1063/1.2263437.

[29] A. 65 United Nations Economic Commission for Europe Regulation 66, "Uniform technical prescriptions concerning the approval of large passenger vehicles with regard to the strength of their superstructure," Geneva, 2006.

Appendix

A 1. Material properties of Mild steel

Elastic properties

Material Property	*Value*
Density	7850 kg/m3
Modulus of elasticity E	210 Gpa
Shear modulus	810 Gpa
Yield strength	235 Mpa
Ultimate strength	360 Mpa
Poisson's ratio	0.3

Plastic property: By using Johnson-cook material model, by ignoring thermal softening effects.

$$\sigma_{eq} = [A + B\varepsilon^{n}] + \left[1 + C \ln \frac{\dot{\varepsilon}}{\dot{\varepsilon}_0}\right]$$

Where, A, B, C and n are constants with values given as

A(MPa)	B(MPa)	n	C
217	233.7	0.6428	0.0756

Johnson-Cook ductile damage model

$$\varepsilon_f = \left[d_1 + d_2 exp(d_3 \left(\frac{\sigma_m}{\sigma_{eq}}\right))\right][1 + d_4 ln(\varepsilon_0)]$$

Where, d_1, d_2, d_3 and d_4 are constants with value given as

d_1	d_2	d_3	d_4
0.1152	1.0116	-1.768	-0.05279

A 2. Crashworthiness test as per ECE-R29 regulation

5. Requirements

5.1. General requirements

5.1.1. The cab of the vehicle shall be so designed and so attached to the vehicle as to eliminate to the greatest possible extent the risk of injury to the occupants in the event of an accident.

5.1.2. Vehicles of categories N_1 and vehicles of categories N_2 with a gross vehicle mass not exceeding 7.5 t shall be subjected to the tests A and C, as described in Annex 3, paragraphs 5. and 7..

However a vehicle type which has been approved according to Regulation No. 33 or to Regulation No. 94 may be considered to have satisfied the requirements on frontal impact (test A).

5.1.3. Vehicles of categories N_3 and vehicles of categories N_2 with a gross vehicle mass exceeding 7.5 t shall be subjected to the tests A, B, and C, as described in Annex 3, paragraphs 5., 6. and 7..

5.1.4. Test A (frontal impact) shall only be conducted on Cab-over-Engine vehicles.

5.1.5. One, two or three cabs, at the manufacturer's choice, may be used for the purpose of demonstrating compliance with paragraphs 5.1.2. or 5.1.3. above. However both phases in test C, if applicable, shall be conducted on the same cab.

5.1.6. None of the tests A, B, C, need be carried out if the manufacturer can show by computer simulation or calculations of the strength of the component parts of the cab or by other means to the satisfaction of the Technical Service that the cab will not undergo deformation dangerous to the occupants (penetration into the survival space) if subjected to the conditions of the tests.

5.2. Survival space required after the test or tests

5.2.1. After undergoing each of the tests referred to in paragraphs 5.1.2. or 5.1.3., the cab of the vehicle shall exhibit a survival space allowing accommodation of the manikin defined in Annex 3, Appendix 2, on the seat, when the latter is in its median position, without contact between the test manikin and non-resilient parts with a Shore-Hardness of 50 or more. No account shall be taken of non-resilient parts which can be moved away without any tools from the test manikin by using a force of less than 100 N. To facilitate installation, the manikin may be inserted in dismantled form and assembled in the cab. For this purpose, the seat shall be adjusted to its most rearward position and the manikin completely assembled and so placed that its H point coincides with the R point. The seat shall then be moved forward to its median position for the assessment of the survival space. As an alternative to the test manikin defined in Annex 3, Appendix 2, a fiftieth percentile Hybrid II or III male dummy, with or without measuring instrumentation, the description of which is given in Regulation No. 94, may be used.

5.2.2. The space so defined shall be verified for every seat provided by the manufacturer.

Test procedure

1. Doors

   Before the tests the doors of the cab shall be closed but not locked.

2. Engine

   For test A the engine, or a model equivalent thereto in mass, dimensions and mounting, shall be fitted to the vehicle.

3. Cab

   The cab shall be equipped with the steering mechanism, steering wheel, instrument-panel and the driver and passenger seats. The steering wheel and the seating position shall be adjusted to their positions for normal use as prescribed by the manufacturer.

4. Anchorage of the cab

   For test A, the cab shall be mounted on a vehicle. For tests B, C the cab shall, at the manufacturer's choice, be mounted either on a vehicle or on a separate frame. The vehicle or frame shall be secured in the manner prescribed in Appendix 1 to this annex.

5. Front impact test (test A)

Figure 1
Front impact test (test A)

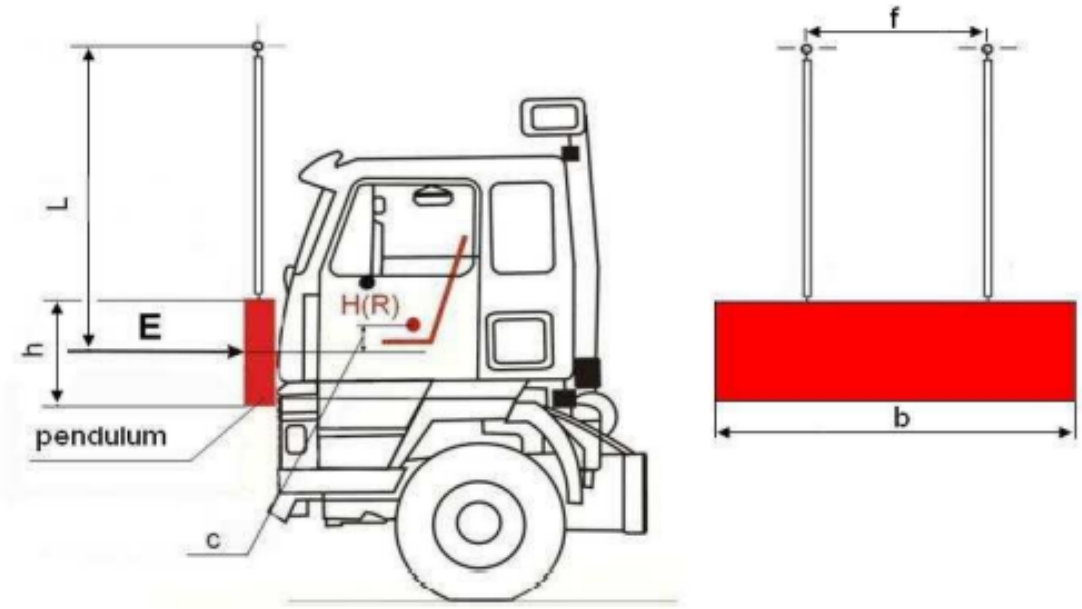

5.1. The impactor shall be made of steel and its mass shall be evenly-distributed; its mass shall not be less than 1,500 kg. Its striking surface, rectangular and flat, shall be 2,500 mm wide and 800 mm high (see b and h on figure 1). Its edges shall be rounded to a radius of curvature of 10 mm± 5 mm.

5.2. The impactor assembly shall be of rigid construction. The impactor shall be freely suspended by two beams rigidly attached to it and spaced not less than 1,000 mm apart (see f on figure 1). The beams shall be not less than 3,500 mm long from the axis of suspension to the geometric centre of the impactor (l on figure 1).

5.3. The impactor shall be so positioned that in the vertical position:

5.3.1. Its striking face is in contact with the foremost part of the vehicle;

5.3.2. Its centre of gravity is c=50 +5/ - 0 mm below the R point of the driver's seat, and

5.3.3. its centre of gravity is in the median longitudinal plane of the vehicle.

5.4. The impactor shall strike the cab at the front in the direction towards the rear of the cab. The direction of impact shall be horizontal and shall be parallel to the median longitudinal plane of the vehicle.

5.5. The impact energy shall be:

5.5.1. 29.4 kJ in the case of vehicles of category N_1 and of vehicles of category N_2 with a gross vehicle mass not exceeding 7.5 t.

5.5.2. 55 kJ in the case of vehicles of category N_3 and of vehicles of category N_2 with a gross vehicle mass exceeding 7.5 t.

A 2. Manikin used to verify survival space to ECE-R29

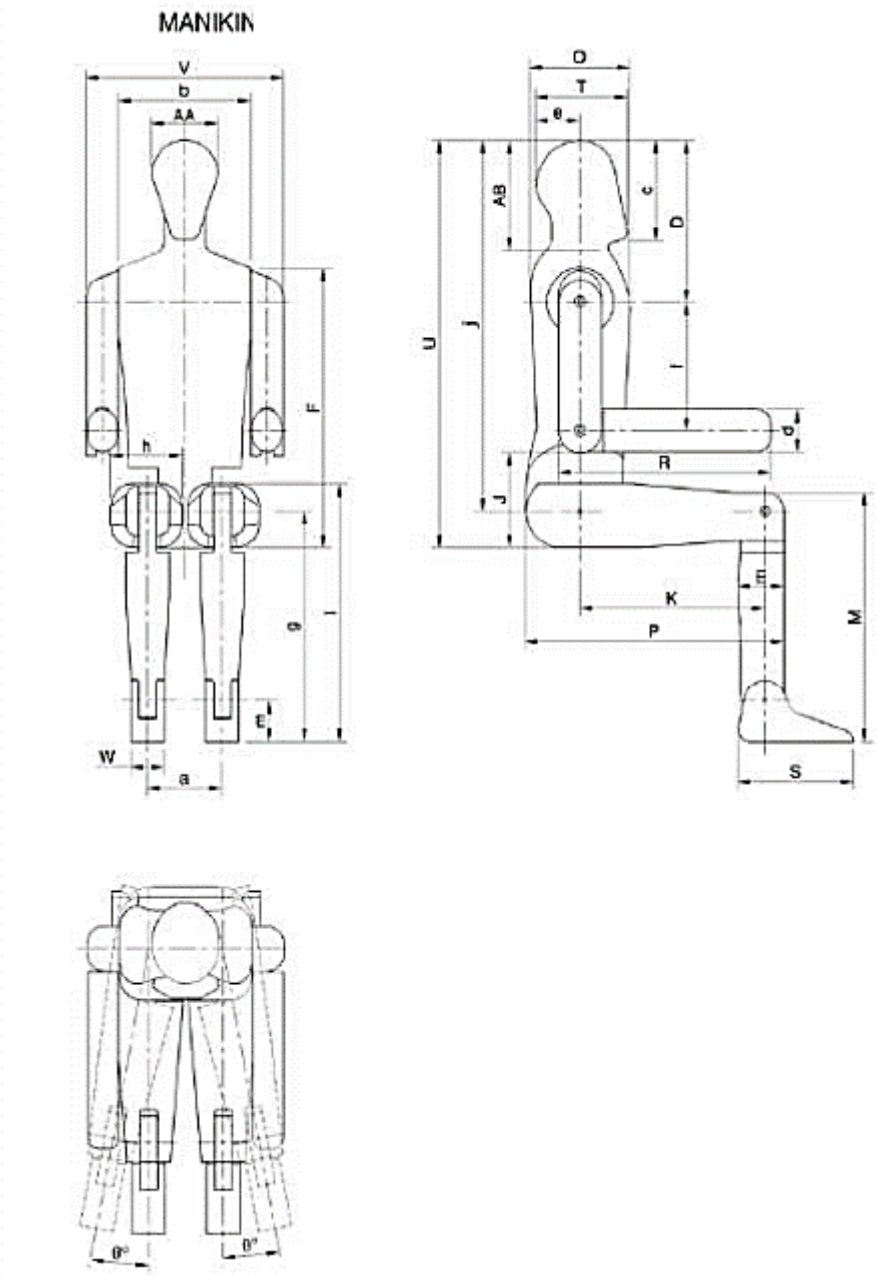

Dimensions of manikin

Dimensions		
Name	*Description*	*Dimension. in mm*
AA	Breadth of head	153
AB	Combined height of head and neck	244
D	Distance from top of head to shoulder pivot	359
E	Calf depth	106
F	Height from seat to top of shoulder	620
J	Height of elbow rest	210
M	Knee height	546
O	Chest depth	230
P	Distance from seat back to knee	595
R	Distance from elbow to fingertip	490
S	Length of foot	266
T	Length of head	211
U	Height from seat to top of head	900
V	Shoulder breadth	453
W	Breadth of foot	77
a	Distance between hip point centers	172
b	Chest breadth	305
c	Height of head and chin	221
d	Forearm thickness	94
e	Distance between vertical centerline of torso and rear of head	102
f	Distance between shoulder pivot and elbow pivot	283
g	Knee pivot height from ground	505
h	Thigh breadth	165
i	Lap height (Sitting)	565
j	Distance from top of head to "H" point	819
k	Distance between hip pivot and knee pivot	426
m	Ankle pivot height from ground	89
θ	Lateral rotation of the legs	20°

A 4. Residual Space Definition as per ECE-R66

Residual space is defined by creating a polynomial within the bus inner frames, which has an outline described in Figures A 4 (a) and A 4 (b), and moving it along the Bus longitudinal center plane. The dimensions and position of residual space is defined according to the following parameters [29]:

1. The SR point is located on the seat-back of each outer forward or rearward facing seat (or assumed seat position), 500 mm above the floor under the seat, 150 mm from the inside surface of the side wall. No account shall be made of wheel arches and other changes of the floor height. These dimensions shall also be applied in the case of inward facing seats in their center planes.
2. If the two sides of the Bus are not symmetric within the floor arrangement and, therefore, the height of the SR points are different, the step between the two floor lines of the residual space shall be taken as the Bus longitudinal center plane (see Figure A 4(b));
3. The rearmost position of the residual space is a vertical plane 200 mm behind the SR point of the rearmost outer seat, or the inner face of the rear wall of the Bus if this is less than 200 mm behind that SR point. The foremost position of the residual space is a vertical plane 600 mm in front of the SR point of the foremost seat (whether passenger, crew, or driver) in the Bus seat at its fully forward adjustment. If the rearmost and foremost seats on the two sides of the Bus are not in the same transverse planes, the length of the residual space on each side will be different;
4. The residual space is continuous in the passenger, crew and driver compartment(s) between its rearmost and foremost plane and is defined by moving the defined vertical transverse plane through the length of the Bus along straight lines through the SR points on both sides of the Bus. Behind the rearmost and in front of the foremost seat SR point the straight lines are horizontal.
5. The manufacturer may define a larger residual space than is required for a given seat arrangement, to simulate a worst case in a group of Bus types to allow for future design development.

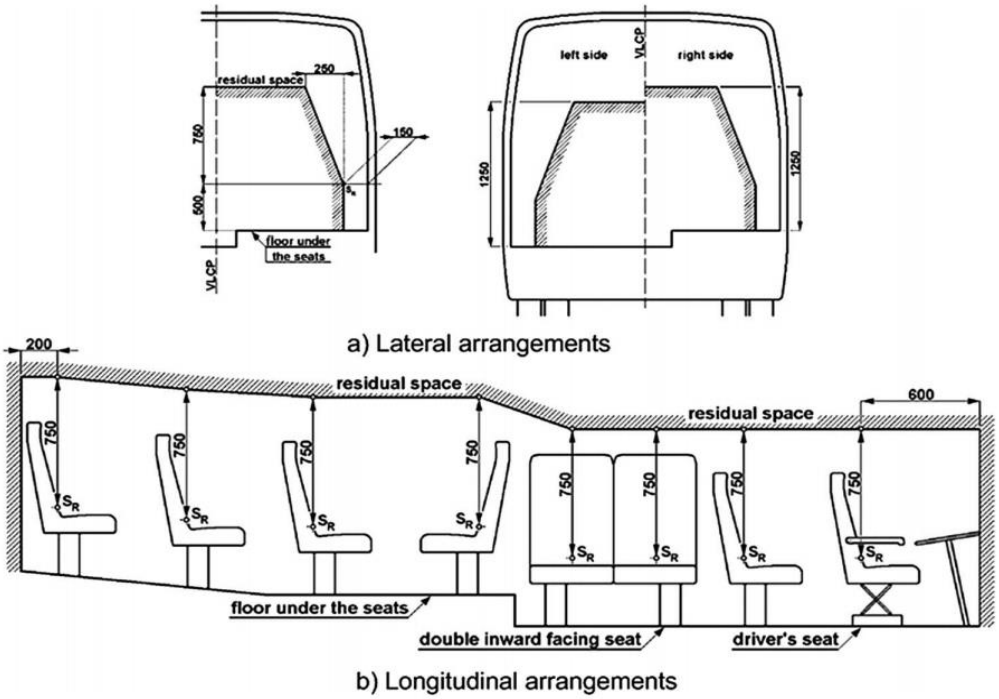

Figure A4. Residual space definition as per ECE-R66